HHS Public Access

Author manuscript

J Bone Miner Res. Author manuscript; available in PMC 2020 September 01.

Published in final edited form as:

J Bone Miner Res. 2019 September ; 34(9): 1690–1706. doi:10.1002/jbmr.3755.

VEGFA from Early Osteoblast Lineage Cells (Osterix+) is Required in Mice for Fracture Healing

Evan G. Buettmann[1,2], **Jennifer A. McKenzie**[1], **Nicole Migotsky**[1,2], **David A.W. Sykes**[3], **Pei Hu**[1], **Susumu Yoneda**[1], **Matthew J. Silva**[1,2]

[1]Department of Orthopaedic Surgery, Washington University in St. Louis

[2]Department of Biomedical Engineering, Washington University in St. Louis

[3]Department of Biology – Washington University in St. Louis

Abstract

Bone formation via intramembranous and endochondral ossification is necessary for successful healing after a wide range of bone injuries. The pleiotropic cytokine, vascular endothelial growth factor A (VEGFA) has been shown, via nonspecific pharmacologic inhibition, to be indispensable for angiogenesis and ossification following bone fracture and cortical defect repair. However, the importance of VEGFA expression by different cell types during bone healing is not well understood. We sought to determine the role of VEGFA from different osteoblast cell subsets following clinically relevant models of bone fracture and cortical defect. Ubiquitin C (UBC), Osterix (Osx), or Dentin Matrix Protein-1 (Dmp1) Cre-ERT2 mice (male and female) containing floxed VEGFA alleles ($VEGFA^{fl/fl}$) were either given a femur full fracture, ulna stress fracture, or tibia cortical defect at 12 weeks of age. All mice received tamoxifen continuously starting two weeks before bone injury and throughout healing. UBC CreERT2 $VEGFA^{fl/fl}$ (UBC cKO) mice, which were used to mimic non-specific inhibition, had minimal bone formation and impaired angiogenesis across all bone injury models. UBC cKO mice also exhibited impaired periosteal cell proliferation during full fracture but not stress fracture repair. Osx CreERT2 $VEGFA^{fl/fl}$ (Osx cKO) mice, but not Dmp1 CreERT2 $VEGFA^{fl/fl}$ (Dmp1 cKO) mice, showed impaired periosteal bone formation and angiogenesis in models of full fracture and stress fracture. Neither Osx cKO nor Dmp1 cKO mice demonstrated significant impairments in intramedullary bone formation and angiogenesis following cortical defect. These data suggest that VEGFA from early osteolineage cells (Osx+) but not mature osteoblasts/osteocytes (Dmp1+) is critical at the time of bone injury

Corresponding Author: Evan G. Buettmann, 601 West Main St., Box 843068, Richmond, VA 23283, Virginia Commonwealth University, Biomedical Engineering, buettmanne@vcu.edu.

Present Affiliations:

Evan Buettmann – Bone Engineering and Science Technology Lab, Department of Biomedical Engineering, Virginia Commonwealth University, Richmond, Virginia

Pei Hu - State Key Laboratory of Oral Diseases, West China Hospital of Stomatology, Sichuan University.

Author Roles:

Study design: MJS, JAM, EGB. Study Conduct: EGB, JAM, NM, DAWS, PH, SY. Data collection: EGB, JAM, NM, DAWS, PH, SY. Data analysis: EGB, JAM, DAWS. Data interpretation: EGB, JAM, MJS. Drafting manuscript: EGB. Revising Manuscript: EGB, JAM, MJS. Approving final version of manuscript: EGB, JAM, MJS. EGB takes responsibility for integrity of data analysis.

Disclosures:

The authors would like to disclose that Matthew Silva has past research grant support from Merck Co. (2014–2017) and occasional royalty income from Springer.

All other authors have no financial conflicts of interest with the submission of this manuscript.

for rapid periosteal angiogenesis and woven bone formation during fracture repair. On the other hand, VEGFA from another cell source, not from the osteoblast cell lineage, is necessary at the time of injury for maximum cortical defect intramedullary angiogenesis and osteogenesis.

Keywords

Injury/Fracture Healing; Osteoblasts; Cytokines; Genetic Animal Models

Introduction:

Bone repair is a complex multi-factorial process that is injury and site specific (1). Rapid bone formation following injury is essential for proper healing. Unfortunately, healing is compromised in 5–10% of all fractures, leading to increased post-injury disability and financial burden (2–8). Therefore, there is substantial motivation to better understand the biological factors influencing new bone formation, which can occur by intramembranous and/or endochondral ossification following bone injury (1, 9–11).

One such factor, vascular endothelial growth factor A (VEGFA), has been shown to be critical to bone formation during repair. VEGFA is a heparin binding pleiotropic cytokine produced by many cell types within the bone microenvironment, including cells of the endothelial and osteochondral lineages (12–20). VEGFA signals predominantly through VEGFR2 (KDR), which functions as a receptor tyrosine kinase and is found on cells of the osteoblast and endothelial lineage within bone (12, 19, 21–24). Previous *in vitro* assays show that exogenous VEGFA promotes human umbilical vein endothelial cell (HUVEC) proliferation, migration and tubule formation (25–27). VEGFA has also been shown to promote *in vitro* osteoblast cell survival, differentiation and mineralization in a dose-dependent manner (15, 22, 28–30). Therefore, VEGFA's role in promoting ossification following bone injury is thought to be due to its role in supporting both angiogenesis and osteoblast function, two processes necessary for bone formation *in vivo* (31–35). However, the nonspecific nature of anti-VEGFA treatments used to block bone repair *in vivo* (32, 36, 37) have not shed light on which cell types are critical sources of VEGFA for this process.

To address this knowledge gap, a recent study showed that constitutively deleting VEGFA from osteoblast lineage cells, using the noninducible Osterix (Osx) Cre, but not from endothelial lineage cells, using the noninducible Cadherin-5 (Cdh-5) Cre, led to impaired intramembranous ossification following tibia defect repair (28). In the same study, the authors also showed that this loss of VEGFA in Osx+ lineage cells impaired angiogenesis at the bone defect site, thereby supporting previously mentioned *in vitro* work. These results demonstrate that VEGFA from Osx+ lineage cells but not Cdh-5+ lineage cells is necessary for angiogenesis and bone formation following cortical defect. However, this study did not address two important questions: 1) Is VEGFA from osteoblast lineage cells critical in more clinically relevant models of bone fracture? 2) Is VEGFA essential in early or later osteoblast lineage cells? VEGFA is highly expressed by osteoblast lineage cells following bone injury (38–41). Its expression has also been shown to increase during osteoblast differentiation and mineralization *in vitro* (22). Therefore, we hypothesized that VEGFA

from both early (Osx+) and later (Dentin Matrix Protein-1, Dmp1+) osteoblast lineage cells is important in clinically relevant fracture repair.

To address these specific questions, we used an inducible Cre_LoxP system in mice harboring VEGFA floxed alleles ($VEGFA^{fl/fl}$) (42). Ubiquitin C (UBC) (43), Osx (44), and Dmp1 (45) inducible Cre-ERT2 lines were crossed to mice carrying floxed $VEGFA^{fl/fl}$ alleles to generate Cre-positive inducible and conditional knockout (cKO) and Cre-negative mice (Control) (Figure 1A). Twelve-week old mice (male and female) underwent either three-point bending of the femur (full fracture) or cyclic axial forelimb compression (stress fracture), two procedures that model clinically relevant fractures that heal by periosteal callus formation. They differ in that full fractures heal by combined intramembranous and endochondral ossification (9, 46, 47), whereas stress fractures heal by intramembranous ossification (48–50). To confirm previous results (28), we also injured bones by drilling of the anterior medial cortex of the tibia (cortical defect). In this model, the predominant site of new woven bone is intramedullary which is formed by intramembranous ossification (51, 52). All mice were given tamoxifen starting 2 weeks before bone injury and throughout healing until sacrifice at predetermined timepoints (Figure 1B).

First, we deleted VEGFA in all cells using the UBC Cre-ERT2 to confirm previous pharmacologic results that global VEGFA is necessary for angiogenesis and osteogenesis following bone injury. Then Osx cKO and Dmp1 cKO mice were used to discern whether VEGFA from early osteoblast lineage cells or more mature osteoblasts/osteocytes is necessary for successful bone repair. Based on previous reports, the inducible Osx Cre-ERT2 would target VEGFA deletion in osteoblast lineage cells from osteoprogenitor to osteocytes (38, 44, 53). On the other hand, the Dmp1 Cre-ERT2 would allow for targeting of only mature osteoblasts and osteocytes (54, 55).

Our results show that UBC+ cell VEGFA is necessary for angiogenesis and osteogenesis across the three models of bone injury. More importantly, we show for the first time that VEGFA from Osx+ but not Dmp1+ cells is necessary for maximal angiogenesis and osteogenesis following full fracture and stress fracture. These data indicate that VEGFA from early osteoprogenitor cells but not mature osteoblasts is critical for rapid periosteal bone formation and angiogenesis following fracture. Finally, we show that cortical defect repair does not depend on VEGFA at the time of injury from Osx+ or Dmp1+ cell lineages. This suggests another cell source of VEGFA is critical for maximal intramedullary bone formation following tibial defect repair.

Materials and Methods:

Mouse Lines –

All mouse lines including UBC Cre-ERT2 (43), Osx Cre-ERT2 (44), Dmp1 Cre-ERT2 (45), Ai9 (RCL-tdTomato) (56), and $VEGFA^{fl/fl}$ (42) were previously generated and described. UBC Cre-ERT2 (Catalog # 007001) and Ai9 (RCL-tdT; Catalog # 007909) breeders were purchased from Jackson Laboratories. Osx Cre-ERT2 and Dmp1 Cre-ERT2 breeders were shared from the laboratories of Drs. Henry Kronenberg and Paola Pajevic, respectively. $VEGFA^{fl/fl}$ breeders were provided by Dr. Bjorn Olsen with permission from Genentech. To

generate inducible Cre reporter mice, male mice hemizygous for Cre were crossed to female mice containing homozygous Ai9 alleles. These offspring were interbred to generate Cre positive mice homozygous for Ai9 that were used separately for Cre specificity and lineage tracing studies. Subsequently, to make VEGFA cKO mice, hemizygous Cre males homozygous for $Ai9^{+/+}$ were bred to female $VEGFA^{fl/fl}$ mice. Mice from each Cre line were then intercrossed to generate the following two genotypes: Cre-ERT2;$VEGFA^{fl/fl}$;Ai9 (cKO) and $VEGFA^{fl/fl}$;Ai9 (Control) for each Cre line (Figure 1A). Mice were group housed (4–5 per cage) under a standard 12-hour light/dark cycle and given access to food (Purina LabDiet 5053, St. Louis, MO) and water ad libitum. All experimental procedures involving animals were approved by the Institutional Animal Care and Use Committee (IACUC) at Washington University in St. Louis School of Medicine in accordance with the Animal Welfare Act (AWA) and PHS Policy on Humane Care and Use of Laboratory Animals.

Mouse Models of Bone Repair –

For all bone repair models the right limb was injured whereas the left contralateral limb served as the uninjured control. Mice were anesthetized during all procedures with isoflurane (1–3% v/v). For invasive procedures (full fracture and cortical defect), mice were given buprenorphine SR (1 mg/kg, s.c.) 1 hr before surgery. The right limb was shaved and sterilized with betadine and alcohol (70%) before surgery. For noninvasive procedures (stress fracture), mice were given Buprenex (0.05 mg/kg, s.c.) immediately following loading. Following all bone injury procedures, mice were returned to their cage and placed on heating pads (Bean Farm) until awake and sternal. Mice were monitored daily for signs of pain and open wounds were quickly resutured.

Full Fracture Model –

Right limbs were prepared before fracture as previously described (47). Briefly, a complete (full) transverse bone fracture was made in the femoral mid-diaphysis via three-point bending using a custom designed fixture on a materials testing machine (DynaMight 8841, Instron). The fracture was stabilized with a 24 gauge stainless steel pin (Microgroup) and the wound sutured with 3–0 nylon sutures (Ethicon). Immediately after fracture, 3x magnification radiographs (Faxitron Ultrafocus 100) were taken to verify proper fixation of the fracture site. Mice were excluded (34 out of 94) if they had an irreparable break (15 mice), loss of fixation during healing (9 mice), signs of infection (3), or processing artifacts (7 mice).

Stress Fracture Model –

Cyclic axial fatigue using a 2 Hz haversine waveform was applied to the right forelimb as previously described (57). Briefly, to ensure equal levels of fatigue-induced damage between experimental groups, each mouse line underwent non-survival calibration loading to determine the ultimate forelimb force (F_{ult}, monotonic loading to failure) and cyclic displacement increase to failure (from cycle 10, D_{10} to D_{fail}). To induce a stress fracture, forelimbs were loaded at a peak force of 75% F_{ult} until displacement reached 50% of the average displacement increase to failure determined from the calibration group (Supplemental Table 3). This resulted in a non-displaced compressive cortical crack visible by micro-CT. Specimens were excluded (56 out of 166) if they had visible cracks spanning

the whole cortex (30 mice), ultradistal fractures through the growth plate (16 mice), or reach displacement limits in under 50 cycles (10).

Cortical Defect Model –

The right tibia was prepared as previously described (51, 58). Briefly, a 0.78 mm circular defect was made using a #68 sterilized drill bit attached to a Dremel tool (Model 395, Bosch Tool Group). It was centered on the anterior medial cortex of the tibia and was located 4.3 mm from the tibial plateau. Following drilling, the cortical defect was irrigated with sterile saline with the wound closed using 5–0 nylon sutures (McKesson). Specimens were excluded (2 out of 47) due to premature death (1 mouse) or drilling through both cortices (1 mouse).

Cre Specificity and VEGFA Colocalization Testing –

In order to determine inducible Cre specificity and VEGFA protein localization during our models of bone fracture repair, male and female mice hemizygous for UBC, Osx, and Dmp1-Cre-ERT2 and containing Ai9 transgenic alleles were used. For this experiment only, control animals contained wild-type VEGFA alleles ($VEGFA^{wt/wt}$) in order to visualize wildtype VEGFA (Alexa-488) and Cre reporter (tdTomato) expression simultaneously. Mice harboring Cre and Ai9 with $VEGFA^{fl/fl}$ alleles served as cKO. To induce Cre activated recombination, mice were administered tamoxifen (TAM) via diet (Envigo; TD.130859) or oral gavage (100mg/kg) starting two weeks before bone injury and throughout healing. Both methods of tamoxifen gave similar Cre activated tdTomato expression patterns during fracture healing. Mice undergoing full fracture were sacrificed at day 14 post-injury. Injured limbs and their contralateral uninjured limbs were fixed in 4% paraformaldehyde (Electron Microscopy Sciences; 15710) for 24 hrs and underwent standard decalcification for 14 days (14% EDTA, pH 7.0) and frozen processing (30% sucrose infiltration followed by embedding and freezing in OCT [Tissue-Tek; 25608–930]). Sections were cut longitudinally at a thickness of 5 μm using the Leica CryoJane Tape Transfer Staining for VEGFA protein was completed on rehydrated sections by immunohistochemistry as previously described (28). In brief, sections were first incubated with 10% goat serum (Abcam; ab7481) for 1 hour at room temperature to block endogenous binding sites. Next, immunostaining for VEGF was performed (Santa Cruz; sc-152 1:50 dilution) overnight at 4°C. For visualization, secondary antibody immunofluorescent incubation (Invitrogen; A-11034; 1:200 dilution) was done for 90 minutes at room temperature. Sections were counterstained with DAPI (Sigma: D9542; 1:1000 dilution) to visualize cell nuclei. Sections were imaged at 20x on a Nanozoomer Slide Scanner (Hamamatsu) with DAPI, TRITC, and FITC channels for nuclear, Cre activated tdTomato, and VEGF Alexa-488 expression, respectively. Final images were exported with NDPView2.0 (Hamamatsu).

VEGFA Deletion Efficiency Testing –

Cre ERT2-$VEGFA^{fl/fl}$;Ai9 (cKO) and $VEGFA^{fl/fl}$;Ai9 (Control) for each Cre line were given TAM by either diet (Envigo; TD.130859) or oral gavage (100 mg/kg) starting 2 weeks before injury and throughout healing as shown in Figure 1B. VEGFA deletion was assessed at the level of DNA (tibia and kidney PCR) and RNA (qPCR of cortical bone from tibia). VEGFA recombination at loxP sites was analyzed by PCR using primers spanning exon 3.

DNA primers (forward - mVEGF322.F [5′-ACTTCATGGACAGGCTTCGG-3′] and reverse - VEGFc5R.2 [5′-ACATCTGCTGTGCTGTAG GAAG-3′]) and cycling conditions have been previously described (59). VEGFA deletion efficiency was quantified by qPCR. Following sacrifice at day 7, tibiae were flushed of marrow and the center third of the diaphysis was snap frozen in liquid N_2. Bones were homogenized, resuspended in Trizol and RNA was extracted and purified using a Qiagen RNeasy Kit. Bioanalyzer (Agilent Technologies) was used to verify RNA integrity (all RIN's > 7) as per MIQE standards (60). Sybr based qPCR was run on a Step One Plus Machine (Applied Biosystems) using the following primers: VEGFA (forward 5′-ATCTTCAAGCCGTCCTGTGT-3′ and reverse 5′-CTGCATGGTGATGTTGCTCT-3′) from within exon 3 (15), Tbp and Ipo8 served as reference genes (IDT Mm.PT.58.42394711, Mm.PT.39a.22214844). Each biological sample was run in triplicate. To determine VEGFA expression, each sample's average VEGFA CT value was subtracted by the average of the CT values from the reference genes (ΔCT); relative expression was computed as 2^-(ΔCT). Note that chow and gavage methods of TAM administration gave similar qPCR VEGFA deletion efficiencies (not shown).

Micro-CT –

Mice were euthanized at previously mentioned timepoints (Figure 1B) and analyzed for bone formation via micro-CT as described by (61). Right (injured) limbs and left (uninjured) limbs were fixed in 10% neutral buffered formalin (Fisher Scientific) for 24 hrs and then prepped for micro-CT. Fractured femurs were scanned in air in a VivaCT 40 system (Scanco Medical) using the following parameters (X-ray tube potential 55 kV, integration time 300 ms, X-ray intensity 145 μA, isotropic voxel size 10.5 μm, frame averaging 1, projections 1000, high resolution scan). Analysis for bone formation was performed using the Scanco software. First, an ROI spanning a 600 slice region (6.3 mm) centered around the fracture site of each femur was contoured (Supplemental Figure 3A). This region covered the majority of the callus. Then, images were unfiltered and thresholded at 183 per mille to segment all mineralized tissue. Stress fractured ulnae and injured tibiae were embedded in 2% agarose and scanned at 10 μm resolution in a Scanco uCT 40 system using the following parameters (X-ray tube potential 70 kV, integration time 300 ms, X-ray intensity 114 μA, isotropic voxel size 10 μm, frame averaging 1, projections 1000, high resolution scan). For stress fractured ulnae, analysis was done on an ROI consisting of the entire woven bone callus excluding the original cortical bone and marrow cavity (Supplemental Figure 3B). For the tibial defect injury model, analysis was done on an ROI spanning the cortical defect (Supplemental Figure 3C). This ROI longitudinally encompassed a 55 slice region (0.55 mm) centered on the defect site of each tibia. All ROI's were drawn and quantified by a blinded user to animal ID and experimental group. Outcome measures for all ROI's included contoured total volume (TV), thresholded bone volume (BV), bone volume fraction (BV/TV), and volumetric bone mineral density (vBMD) as previously described (47). 3D reconstructions of full fractured femurs and stress fracture ulnae were created by importing DICOM stacks of the analysis region into Dragonfly bone 3D software (Object Research Systems). 3D reconstructions of cortical defect tibiae were created within the Scanco software suite.

Histology and Histomorphometry –

Following micro-CT, specimens underwent decalcification for 14 days (14% EDTA, pH 7.0) followed by standard paraffin processing. Injured femurs and tibia were then sectioned at 5 μm longitudinally near the middle of the fracture callus or defect site, respectively. Injured ulnae were sectioned at a 5 μm thickness transversely near the fracture line. Serial sections were stained with picrosirius red alcian blue (PRAB; full fracture) or hematoxylin and eosin (H&E; stress fracture and tibial defect) or left unstained for immunohistochemistry. PRAB and H&E sections were imaged at 20x and 40x, respectively, on a Nanozoomer Slide Scanner (Hamamatsu). For fractured femurs and ulnae, the total callus, cartilage and woven bone areas were quantified by a blinded user to mouse ID and experimental group 3x and presented as previously described (62). Other tissue within the callus not classified as cartilage or woven bone was called periosteal fibrous tissue. The relative proportion of each of these three tissue types is presented as a percentage of the total callus area (adding up to 100%). Fractured femurs were analyzed by the Nanozoomer software (NDP viewer, Hamamatsu). Fractured ulnae were analyzed by the software BIOQUANT (Nashville, TN). Specific histomorphometric nomenclature were used as described in (63).

Cell Proliferation –

Cell proliferation was assessed by immunohistochemistry (IHC) for proliferating cell nuclear antigen (PCNA, Invitrogen Systems Kit 93–1143) on paraffin sections from full fracture (Day 5) and stress fracture (Day 3). At least one negative control section (incubated without primary antibody) was run per batch using the same procedures. For full fracture analysis, two 20x fields of view that were 1 mm and 2 mm from the fracture site for each specimen were analyzed by the IHC Image Analysis Toolbox plugin (64) on FIJI (65). First, the cortical bone and surrounding skeletal muscle was removed so that just cells in the expanded periosteum were visible. Second, positive pixel intensities representing “positive DAB nuclei” were selected from all images in a set to build a color detection threshold. Third, nuclei segmentation parameters were set to a window size of 15 pixels and seed size of 100 pixels. Fourth, positive nuclei were automatically detected in all sample images using this color threshold and segmentation regimen. Lastly, the number of number of positive nuclei divided by the expanded periosteal area (defined as the area between the cortical bone and skeletal muscle) was calculated to define the periosteal proliferation density (# $PCNA^+$ cells/periosteal area (mm^2)). A similar protocol was followed for stress fracture analysis except this time 10x fields of view encompassing the whole expanded periosteal region were uploaded.

Angiogenesis –

Vascularity was analyzed at Day 5 and Day 14 for full fracture by quantifying blood vessels in high powered fields (20x) of the expanded periosteum that were 1 mm and 2 mm from the fracture site. For the stress fracture model, blood vessels in the entire expanded periosteal callus (area between cortical bone and skeletal muscle) was quantified at Day 3, Day 5, and Day 7. Vessels were visualized using immunohistochemistry with a rat monoclonal endomucin (clone eBioV.7C7, ebisocience; 1:400 dilution) antibody on paraffin sections. Continuous structures that were $endomucin^+$ were counted as blood vessels. Sections

underwent standard IHC paraffin protocols including deparaffinization in xylene and rehydration in graded ethanols. Antigen retrieval was done by proteinase K (5 min, room temp) with subsequent processing done according to the Vectastain Elite ABC HRP kit (Vector Labs; PK-6104). At least one negative control section was run per batch using the same procedures but with an isotype control antibody (Clone eBR2a, ebioscience; 1:400 dilution). Detection was done with ImmPact DAB Peroxidase (HRP) Substrate (Vector Labs; SK-4105). Sections were imaged at 20x on a Nanozoomer Slide Scanner (Hamamatsu) and analyzed by a blinded user to mouse ID and experimental group.

Callus Resorption –

Osteoclast activity was assessed by tartrate-resistant acid phosphatase (TRAP) staining of full fracture (day 14) and stress fracture (day 7) paraffin sections. For full fracture quantification, high powered (20x) sections 1 mm and 2 mm from the fracture site, were analyzed by a blinded user. Multinucleated TRAP+ osteoclast number (N.Oc) and length (Oc.S) were counted via the cell counter plugin and the tracing function respectively on FIJI (65) and normalized by woven bone surface (BS) as reported previously (63). Stress fracture specimens regardless of genotype had no multinucleated TRAP+ osteoclasts on woven bone surfaces and therefore were not quantitated.

Statistics –

Sample sizes for each experimental outcome were calculated *a priori* based on a power analysis with $\alpha = 0.05$ and $\beta = 0.20$. Estimates of sample variance and effect size was based on previous experimental data and biological importance respectively. Target samples sizes for outcomes per experimental group were as follows: qPCR: n = 6; MicroCT n = 8; Histology: n = 6. Every effort was made to equally distribute male and female mice across experimental groups for each outcome measure. Actual sample sizes are visible in the results, directly within all figures. Data are presented as mean ± SD and were analyzed via GraphPad Prism Pro Software (Version 7; La Jolla, Ca). Due to differences in background strain, direct comparisons of quantitative data of the two experimental groups (VEGFA cKO vs. control) were only done within each Cre line. First, datasets were checked for normality and then equal variance using the Shapiro-Wilk normality test and F test, respectively. If datasets passed both of these conditions, they were then compared with an unpaired *t-test.* If either condition failed, datasets were compared with the nonparametric Mann-Whitney test. Full fracture proliferation and vascular data were analyzed by a 2-way repeated measures ANOVA for the effects of genotype, location, and interaction. Sidak's post-hoc test was used to correct for multiple comparisons. Stress fracture proliferation and vascular data were compared by a 2-way ANOVA for the effects of genotype, timepoint, and interaction. Sidak's post-hoc test was used to correct for multiple comparisons. P values of < 0.10 were considered trending while p values of < 0.05 were considered significant.

Results:

Inducible Cre Lines Show Differential Efficiencies for VEGFA Deletion and Spatial Targeting of the Fracture Callus

In order to test the utility of UBC, Osx, and Dmp1 inducible Cre lines for deletion of VEGFA, we first assessed tail snip DNA for recombination. Only after 2 weeks of tamoxifen exposure was recombination via gel electrophoresis apparent in each mouse Cre line (data not shown). Therefore, a tamoxifen induction period of 2 weeks was used before bone injury. UBC cKO mice demonstrated VEGFA recombination in kidney and tibial DNA (Supplemental Figure 1A), whereas Osx cKO and Dmp1 cKO demonstrated VEGFA recombination only in DNA from the tibia. qPCR of mRNA from diaphyseal cortical bone following 3 weeks of tamoxifen exposure demonstrated that all three inducible Cre drivers could downregulate VEGFA mRNA expression (Supplemental Figure 1B). UBC cKO showed a dramatic and significant reduction in VEGFA expression (−96%) compared to littermate controls. In addition, Osx cKO and Dmp1 cKO showed significant and similar levels of downregulation of VEGFA expression (−34%) compared to littermate controls.

To determine inducible Cre specificity in UBC, Osx, and Dmp1 Cre-ERT2 fracture calluses, 12-week old Cre+ mice carrying the Ai9 allele (56) and wildtype VEGFA alleles ($VEGFA^{wt/wt}$) were subjected to full fracture or stress fracture with tamoxifen dosing before and throughout fracture healing. Full fractured mice were also immunofluorescently co-stained for VEGFA to determine protein localization with Cre reporters during fracture healing. Subsequently, full fractured Cre+ Ai9 mice with $VEGFA^{fl/fl}$ were used to verify spatial VEGFA deletion in callus tissues following Cre activation. First, uninjured limbs of UBC;Ai9;$VEGFA^{wt/wt}$ mice showed broad targeting of skeletal tissues with tdTomato expression (indicating Cre recombination) in cortical bone, marrow and muscle (Figure 2A). In contrast, Osx;Ai9;$VEGFA^{wt/wt}$ and Dmp1;Ai9;$VEGFA^{wt/wt}$ uninjured limbs showed tdTomato expression that was more confined to cortical bone. Fractured femurs from UBC;Ai9;$VEGFA^{wt/wt}$ mice showed targeting of all newly formed callus tissues at day 14, with tdTomato expression in woven bone and cartilage along the transition zone. Osx;Ai9;$VEGFA^{wt/wt}$ fractured femurs showed tdTomato expression within the woven bone and cartilage tissues at the transition zone, but not within the muscle. Dmp1;Ai9;$VEGFA^{wt/wt}$ fractured femurs also had tdTomato expression within the woven bone. In contrast, Dmp1; Ai9+ fractured femurs showed tdTomato expression in muscle cells but not in the cartilage region of the callus. Fluorescent immunostained sections from Cre-ERT2;Ai9;$VEGFA^{wt/wt}$ fractured femurs demonstrated that the majority of VEGFA protein was localized within the woven bone regions of the callus (Figure 2B). This VEGFA was also highly co-localized with tdTomato UBC+, Osx+ and Dmp1+ lineage cells. Importantly, immunostained sections from all Cre-ERT2;Ai9;$VEGFA^{fl/fl}$ fractured femurs showed markedly reduced VEGFA within woven bone regions of the callus versus Cre-ERT2;Ai9;$VEGFA^{wt/wt}$ fractured femurs. VEGFA protein was also present to a small degree in some cartilage and muscle cells, but was not present in Cadherin-5 Cre-ERT2 activated tdTomato+ endothelial cells (data not shown). Stress fractured limbs showed similar tdTomato expression patterns in cortical bone and woven bone callus tissue (Supplemental Figure 2).

Deletion of VEGFA Ubiquitously and in Early (Osx+) but not Later (Dmp1+) Osteolineage Cells Impaired Periosteal Bone Formation after Full Fracture and Stress Fracture

In order to determine the effects of UBC, Osx, and Dmp1 driven deletions of VEGFA on full fracture bone formation (endochondral + intramembranous ossification), micro-CT was performed on day 14 fracture calluses. Visualization and quantification of the full fracture showed that femurs from the three control Cre lines produced robust and similar amounts of bone callus 14 days after injury (Figure 3A-B, white bars; ROI in Supplemental Figure 3A). However, healing was visibly and quantitatively altered in UBC cKO and Osx cKO. First, UBC cKO calluses showed a significant and dramatic impairment in bone volume (BV; −48%). Osx cKO calluses also showed a significant albeit not as severe impairment in bone volume (−27%), compared to controls. Contrary to our hypothesis, Dmp1 cKO calluses showed no differences in bone volume compared to controls despite similar deletion efficiency of VEGFA as Osx cKO at baseline. These micro-CT results were reinforced when we examined hematoxylin and eosin (H&E) as well as serial picrosirius red/alcian blue (PRAB) stained sagittal sections at the fracture midpoint from the same mice (Figure 3B-C). Control calluses displayed a mixture of woven bone around the periphery of the fracture and cartilage at the fracture site, confirming that this model heals by combined intramembranous and endochondral ossification. Calluses from UBC cKO fractured femurs trended toward being smaller (−39%; $p = 0.06$) compared to control mice. Furthermore, these smaller UBC cKO fracture calluses had a significantly decreased percentage of woven bone with relative increases in cartilage and fibrous tissue callus area fractions versus controls. Although Osx cKO fracture calluses had less absolute woven bone, this scaled with callus size resulting in no changes in woven bone area fraction versus controls. Dmp1 cKO mice showed no decreases in callus size or composition versus controls. Further quantification of multinucleated TRAP+ woven bone lining osteoclasts from full fracture callus serial sections at day 14 demonstrated that the decreased woven bone formation in UBC cKO and Osx cKO fractured femurs was not due to altered osteoclast abundance (Supplemental Figure 4A).

To look solely at an intramembranous mechanism of healing we performed fatigue loading to produce a stress fracture. On average, in all mouse strains, it took > 3000 cycles to produce a stress fracture (Supplemental Table 1). The resulting periosteal woven bone was quantified one week following stress fracture and generally mirrored results seen in the full fracture model (Figure 4, ROI in Supplemental Figure 3B). Ulnae from the three control Cre lines demonstrated robust periosteal woven bone formation that was localized around the stress fracture (Figure 4A). UBC cKO ulnae showed no quantifiable bone formation as assessed by micro-CT. Osx cKO calluses showed a significant reduction in bone volume (BV; −54%) versus controls. The smaller BV in Osx cKO ulnae was due in part to significantly less bone along the length of the ulna (bone extent; −40%; data not shown). Dmp1 cKO calluses showed no differences in bone metrics compared to controls via micro-CT. H&E stained transverse sections from the same stress fractures illustrated a region of woven bone and expanded periosteum (E.Ps) near the crack in all Cre lines (Figure 4B). Histomorphometry quantification found lower callus area in UBC cKO (−39%), Osx cKO (−31%), and Dmp1 cKO (−43%) ulnae, however these differences reached significance only for the Dmp1 cKO. Due to similar reductions in total volume and bone volume, bone area

fraction of the callus was not significantly altered in UBC, Osx, or Dmp1 cKO mice versus controls. Quantification of TRAP+ multinucleated cells on day 7 serial histological sections demonstrated no osteoclasts lining woven bone surfaces, indicating that the smaller woven bone formation found via micro-CT in UBC and Osx cKO stress fractured ulnas versus controls was not likely due to altered osteoclast abundance (Supplemental Figure 4B). However, the absence of a large relative cartilage area per callus area following stress fracture confirmed that this model healed predominantly by intramembranous ossification unlike the full fracture model.

Deletion of VEGFA Ubiquitously but not in Early (Osx+) Osteolineage Cells Impairs Periosteal Proliferation after Fracture

Cellular periosteal proliferation is a hallmark of the bone injury response to fracture and is necessary for maximal bone formation (66–68). To determine if the reduced bone formation in UBC cKO and Osx cKO was due to impaired cellular proliferation, the expanded periosteal layer of full and stress fracture calluses at day 5 and day 3, respectively, were stained with proliferating cell nuclear antigen (PCNA, Figure 5). First, regardless of bone injury type there was positive PCNA staining providing evidence for cellular proliferation in all control and conditional knockout calluses (Figure 5A;5B). However, proliferation density (# $PCNA^+$ cells/mm^2) was on average an order of magnitude higher in full fracture versus stress fracture expanded periosteal layers, which correlates with the relative magnitudes of periosteal bone formation between the two models. In the full fracture model, it was noted that cellular proliferation appeared heterogeneous within the expanded periosteum and therefore two periosteal locations, 1 and 2 mm from the fracture site, were analyzed for proliferation density. UBC cKO femur calluses demonstrated significantly lower proliferation density near the fracture site (−60%; 1 mm; Figure 5A) versus controls. This effect was not observed further from the fracture site (2 mm region). This impairment in cellular proliferation coincides with the trending decrease in callus area seen in UBC cKO day 14 full fracture calluses versus controls (−39%; Figure 3B). Osx femurs showed no significant differences in cellular proliferation based on genotype or location in the full fracture model. In the stress fracture model, proliferation density of the entire expanded periosteum, the area between the fractured cortical bone and skeletal muscle, was not significantly different in UBC cKO or Osx cKO ulnae calluses versus controls (Figure 5B).

Deletion of VEGFA Ubiquitously and in Early (Osx+) Osteolineage Cells Impairs Periosteal Angiogenesis Following Full Fracture and Stress Fracture

Angiogenesis is a prerequisite for bone formation in models of full fracture and stress fracture repair (21, 31, 33, 69). Since VEGFA is the prototypical angiogenic factor, we assayed whether the reduced periosteal bone formation in UBC and Osx cKO calluses was due to impairments in post fracture angiogenesis at timepoints preceding and concurrent with osteogenesis. At day 5 after full fracture, before robust osteogenesis, the tissues in the expanded periosteal layer of all calluses (control and cKO) were highly vascularized (Figure 6A). For example, there were no significant impairments in vessel density (# endomucin $^+/mm^2$) of the expanded periosteal layer in UBC cKO and Osx cKO femurs compared to controls at either 1 mm or 2 mm locations from the fracture site. By day 14 however, there was a large detectable impairment in the vessel density of cKO callus tissues. For example,

there was a significantly lower vessel density in UBC cKO (−76%; Figure 6B; 1mm) and Osx cKO (−53%; Figure 6B; 1mm) callus tissues versus controls. This effect may be due in part to changes in callus tissue type at the 1 mm site, where UBC cKO displayed predominantly cartilage and Osx cKO displayed transitional tissue, compared to predominantly woven bone in controls. However, looking strictly within woven bone tissue at the 2 mm site, vessel density was still significantly impaired in UBC cKO (−50%) and Osx cKO (−25%). Following stress fracture, there was significantly reduced callus vessel density due to UBC cKO (−22%; Figure 7) of VEGFA versus controls. Osx cKO only showed decreased callus vessel density at day 3 (−38%; Figure 7A) but not day 7 (Figure 7B) versus controls. When looking solely within woven bone tissue, UBC cKO calluses again displayed a strong and significant reduction in woven bone vessel density at day 5 and day 7 (−90%; Supplemental Table 2). Although Osx cKO calluses displayed lower woven bone vessel densities (Supplemental Table 2) than controls at these same timepoints, this result didn't reach significance.

Deletion of VEGFA Ubiquitously but not in Early (Osx+) or Late (Dmp1) Osteolineage Cells Impaired Cortical Defect Repair

To extend our results from the stress fracture model to another model of intramembranous bone formation (51, 52), as well as compare to previously published results (28), we performed a cortical defect in the tibia of UBC, Osx and Dmp1 cKO mice. In contrast to both fracture models that showed robust periosteal bone formation, the cortical defect model only showed intramedullary woven bone formation localized near the defect site (Figure 8F). A week following drilling of the anterior-medial face of the tibia, all control tibiae showed infilling of the cortical defect ROI regardless of background strain (Figure 8A–8B, ROI in Supplemental Figure 3C). UBC cKO demonstrated significantly less bone within the defect site compared to control (−75% BV; Figure 8C). However, unlike in the full fracture and stress fracture injuries where loss of VEGFA from Osx+ cells inhibited bone formation, Osx cKO had normal defect healing. Dmp1 cKO also had normal defect healing. Histological H&E and endomucin stained sections also qualitatively demonstrated impaired woven bone (Figure 8D) and vasculature (Figure 8E) across the defect site in UBC cKO defects. On the other hand, Osx cKO and Dmp1 cKO tibiae demonstrated normal bone formation and vasculature at the defect site.

Discussion:

VEGFA, due to its strong affinity to promote angiogenesis, has been previously studied in the context of bone repair, a process that requires angiogenesis (31, 69). In this study, we tested the requirement of VEGFA from all cells and then from various osteolineages for successful healing in multiple models of bone injury. Our short-term deletion strategy did not cause any observable complications or adversely affect cortical bone properties (Supplemental Table 3), thereby allowing us to look at VEGFA's role in injury induced ossification without a major underlying phenotype.

Overall, we showed that global loss of VEGFA dramatically impairs angiogenesis and osteogenesis in models of full fracture, stress fracture, and cortical defect healing (Figure 9).

More importantly, our results show for the first time that VEGFA from osteoprogenitors/early-stage osteoblasts (Osx+), but not from more mature osteoblasts/osteocytes (Dmp1+), is necessary for maximal periosteal osteogenesis after both full fracture and stress fracture (Figure 9A). Thus, Osx+ cellular VEGFA is a prominent signaling molecule supporting periosteal angiogenesis and osteogenesis necessary for successful full fracture and stress fracture repair. In partial contrast to the results for periosteal bone healing, both Osx+ and Dmp1+ cellular VEGFA were dispensable for intramedullary bone formation during cortical defect repair (Figure 9B). Taken together, these results only partial support our hypothesis that both Osx+ and Dmp1+ cellular VEGFA are important for successful bone repair, and thus highlight the cell lineage and injury specific requirement of VEGFA for bone healing.

We showed that UBC cKO cortical bone demonstrated a potent decrease in VEGFA gene expression and protein production within the bone injury microenvironment that resulted in a dramatic decrease in post injury angiogenesis and osteogenesis across all injury models. To our knowledge, this is the first study to globally delete VEGFA using a genetic approach. Our results support previous *in vivo* studies that used soluble, neutralizing antibodies to block VEGFA signaling during bone repair (32, 37). These studies also showed a dramatic decrease in angiogenesis and osteogenesis that results in impaired healing. These results as well as our own highlight the global importance of VEGFA for the processes of angiogenesis and osteogenesis critical to bone repair.

Furthermore, we showed that Osx cKO but not Dmp1 cKO of VEGFA impaired periosteal osteogenesis in two models of fracture. Even though the deletion efficiencies of VEGFA expression in cortical bone from Osx cKO and Dmp1 cKO mice were similar (Supplemental Figure 1B), and even though both Cre's downregulated VEGFA protein in the woven bone callus (Figure 2B), our results indicate that VEGFA is only indispensable from early osteoprogenitor cells (Osx+) and not mature osteoblasts or osteocytes (Dmp1+). Therefore. we propose that during fracture repair VEGFA may function more to support osteoblast differentiation rather than mature osteoblastic bone apposition. This is supported by recent studies that show VEGFA deletion in constitutive Osx Cre mice impairs *in vitro* and *in vivo* osteoblastogenesis during long bone development (70) and repair (28). Importantly, we also showed that the decreased bone formation in Osx cKO mice versus controls is not due to enhanced bone turnover at early bone formation timepoints since osteoclast surface and number on newly formed woven bone surfaces were not significantly altered in day 14 full fracture or day 7 stress fracture repair (Supplemental Figure 4). In addition, we showed that Osx cKO of VEGFA impaired periosteal angiogenesis following full fracture (Figure 6). This was especially true at timepoints concurrent with osteogenesis such as day 14. This provides strong evidence that VEGFA from Osx-lineage cells is a chemotactic signal for vascular infiltration of the callus. This effect has been described previously, where Osx:GFP (pre-osteoblast) but not Col1:GFP (mature osteoblast) cells were show to co-invade developing long bones with CD31 positive vessels (38). Maes et al. noted that Osx+ osteoblast precursors but not Col1+ mature osteoblasts may be directly driving vascular invasion; our data affirms the author's hypothesis, showing that VEGFA from Osx+ cells promotes vascular invasion necessary for periosteal osteogenesis.

Ubiquitous deletion of VEGFA (UBC cKO) during full fracture healing resulted in smaller calluses made up of primarily cartilage and fibrous tissues (Figure 3C). Consistent with the smaller callus, UBC cKO mice showed a decrease in periosteal cellular proliferation near the fracture at a site that readily undergoes endochondral ossification (1 mm; Figure 5A). Although VEGFA signaling has been shown to be important for chondrocyte survival and differentiation (13, 36, 71), our UBC cKO full fracture calluses demonstrated elevated relative amounts of cartilage compared to controls, with chondrocytes that appeared hypertrophic at day 14 via morphology (Figure 3B;3C). Therefore, it appears that cartilage formation is not impaired due to loss of VEGFA, and that the relative lack of bone in UBC cKO full fracture calluses is likely due to the impaired vascular invasion necessary for endochondral ossification rather than a failure to form cartilage callus. In support of this, impaired endochondral ossification marked by cartilage tissue accrual was seen in the growth plate and fracture calluses of mice treated with pharmacological inhibitors that block VEGFA signaling (32, 34, 72). Similarly, inhibition of VEGF signaling blocked endochondral ossification of fetal bone and skeletal stem cell transplants without impairing chondrogenesis (73). In addition, previous fracture studies showing decreased angiogenesis have also demonstrated impaired periosteal proliferation (33, 69, 74, 75). Collectively, these data indicate that VEGFA, by promoting periosteal angiogenesis and proliferation, supports endochondral ossification necessary for full fracture repair.

In contrast to endochondral ossification, intramembranous ossification occurs without a cartilage intermediate and is the predominate ossification mechanism of periosteal bone formation in stress fractures (9, 48, 50, 76). Our stress fracture model showed little to no cartilage formation (Figure 4B), and thus allowed us to determine the role of cellular VEGFA in periosteal intramembranous healing. Loss of VEGFA in Osx cKO but not Dmp1 cKO impaired osteogenesis at day 7 in the healing stress fracture (Figure 4A) without alterations in osteoclast number (Supplemental Figure 4B), which indicates that VEGFA from early osteoprogenitor (Osx+) cells is crucial for *de novo* periosteal intramembranous ossification. Osx cKO of VEGFA also showed impaired periosteal angiogenesis (Figure 7), but not cellular proliferation (Figure 5B), both of which are necessary for stress fracture repair (31, 48, 76). These results are consistent with the view that VEGFA's primary role is to recruit periosteal vasculature necessary for intramembranous ossification of the stress fracture callus.

Lastly, we show that that UBC cKO but not Osx or Dmp1 cKO of VEGFA impairs osteogenesis associated with repair of a cortical defect (Figure 8A;8B). Osteogenesis following cortical defect occurs predominantly through an intramembranous mechanism since there is little to no cartilage at the site of new bone formation (50, 51, 57, 77). Histologically, the new bone appears to derive from the bone marrow (Figure 8D;8E). Moreover, we showed that removal of the periosteum does not impede cortical defect healing (Supplemental Figure 5), although others have shown it does block full fracture repair (66, 67). This suggests that the bone forming osteoblasts during cortical defect repair are not derived from the periosteum but instead are likely from progenitor cells in the endocortical or marrow spaces (intramedullary). This is further supported by the fact that UBC;Ai9 mice show more tdTomato targeting of marrow cells than either Osx;Ai9 or Dmp1;Ai9 (Figure 2A) and that VEGFA from UBC+ cells but not Osx+ cells is necessary

for cortical defect repair. Overall, these results highlight the injury specific requirement of cellular VEGFA since it is required in Osx+ lineage cells for maximal periosteal osteogenesis but not intramedullary osteogenesis.

Our study had several limitations. First, our Osx and Dmp1 cKO mice showed modest deletion efficiencies in uninjured cortical bone compared to others (Supplemental Figure 1B). Liu et al., using the noninducible Osx Cre showed a 70% knockdown of VEGFA in diaphyseal cortical bone (15). However, we observed a clear, localized reduction in VEGFA protein in the woven bone regions of the fracture callus of UBC, Osx, and Dmp1 cKO mice versus controls. Whether a more efficient knockdown in our Osx cKO mice would have led to more robust impairments in angiogenic and osteogenic outcomes remains to be determined, but it is possible that the importance of VEGFA from Osx-expressing cells may be underestimated in the current study. Importantly we note that even with similar deletion efficiencies in cortical bone we did see differences in bone formation responses between Osx and Dmp1 cKO mice. A second limitation is that Osx;Ai9;VEGFA$^{wt/wt}$ mice showed Cre activation in hypertrophic chondrocytes that also stained positive for VEGFA during full fracture repair (Figure 2B). Therefore, the partial impairment in full fracture repair using Osx cKO mice may also be due to loss of VEGFA in hypertrophic chondrocytes. Deletion of VEGFA using a chondrocyte-specific Cre would be needed to address this possibility. Nonetheless, our findings of reduced periosteal bone formation after stress fracture, and of reduced periosteal vasculature in the regions of intramembranous bone formation after full and stress fracture, indicate that VEGFA from osteoblast lineage cells is essential. A third limitation is that our continuous tamoxifen dosing schedule ensured that VEGFA was deleted throughout the entire timecourse of bone repair. We did this to achieve maximal Cre-ERT2 activation in each mouse line and to ensure that each cellular source of VEGFA first was important for bone repair. However, previous results have suggested that there may be a critical timeframe for angiogenesis following fracture in order to prevent delayed healing/nonunion (33, 78). Therefore, future work is needed to determine the temporal requirement of VEGFA for successful repair.

In conclusion, our UBC cKO results support the role of nonspecific VEGFA in angiogenic and osteogenic processes during bone repair. More importantly, the consistent results showing impaired periosteal angiogenesis and periosteal osteogenesis in both the full fracture and stress fracture models indicate that early osteoprogenitors (Osx+) but not mature osteoblast lineage cell (Dmp1+) VEGFA is critical in supporting periosteal angiogenesis and bone formation. This however is not the case during tibial defect repair, where VEGFA from Osx+ lineage cells is dispensable for intramedullary bone formation. These novel results highlight the cellular and injury specific role that VEGFA plays during bone repair and thus may aid in the development of future bone fracture therapies.

Supplementary Material

Refer to Web version on PubMed Central for supplementary material.

Acknowledgements:

This work was supported by funding from NIAMS (R01 AR050211 and P30 AR057235). The authors would like to thank the Washington University in St. Louis Musculoskeletal Research Center (MRC) Cores and staff for assistance. Thanks to Dan Leib for training and assistance in Xray (Faxitron) and micro-CT (Scanco) image acquisition and analysis. Many thanks to Crystal Idleburg and Samantha Coleman for histological processing and sectioning of all bone repair specimens. Thanks to Dr. Michael Ross from the Weilbacher Laboratory (Washington University School of Medicine) for supplying protocols and assistance with endomucin staining. Histological images were taken with the Nanozoomer at Alafi Neuroimaging Core (S10 RR027552). VEGFA$^{fl/fl}$ mice from Genentech were kindly provided by the lab of Bjorn Olsen (Harvard). Inducible Osx Cre-ERT2 were kindly provided by the lab of Henry Kronenberg (Harvard). Inducible Dmp1 Cre-ERT2 from Paolo Pajevic (Boston University) were kindly provided by the lab of Alexander Robling (Indiana University Medical School).

Grant Supporters: NIAMS (R01 AR050211 and P30 AR057235).

References:

1. Einhorn TA, and Gerstenfeld LC. Fracture healing: mechanisms and interventions. Nature reviews Rheumatology. 2015;11(1):45–54. [PubMed: 25266456]
2. Woolf AD, and Pfleger B. Burden of major musculoskeletal conditions. Bulletin of the World Health Organization. 2003;81(9):646–56. [PubMed: 14710506]
3. Tzioupis C, and Giannoudis PV. Prevalence of long-bone non-unions. Injury. 2007;38 Suppl 2:S3–9.
4. Johansen A, Evans RJ, Stone MD, Richmond PW, Lo SV, and Woodhouse KW. Fracture incidence in England and Wales: a study based on the population of Cardiff. Injury. 1997;28(9–10):655–60. [PubMed: 9624346]
5. Gaston MS, and Simpson AH. Inhibition of fracture healing. The Journal of bone and joint surgery British volume. 2007;89(12):1553–60. [PubMed: 18057352]
6. Dimitriou R, Jones E, McGonagle D, and Giannoudis PV. Bone regeneration: current concepts and future directions. BMC medicine. 2011;9:66. [PubMed: 21627784]
7. Dickson K, Katzman S, Delgado E, and Contreras D. Delayed unions and nonunions of open tibial fractures. Correlation with arteriography results. Clinical orthopaedics and related research. 1994(302):189–93.
8. Bonafede M, Espindle D, and Bower AG. The direct and indirect costs of long bone fractures in a working age US population. Journal of medical economics. 2013;16(1):169–78. [PubMed: 23035626]
9. Marsell R, and Einhorn TA. The biology of fracture healing. Injury. 2011;42(6):551–5. [PubMed: 21489527]
10. Einhorn TA. Enhancement of fracture healing. Instructional course lectures. 1996;45:401–16. [PubMed: 8727759]
11. O'Keefe RJ. Fibrinolysis as a Target to Enhance Fracture Healing. The New England journal of medicine. 2015;373(18):1776–8. [PubMed: 26510027]
12. Neufeld G, Cohen T, Gengrinovitch S, and Poltorak Z. Vascular endothelial growth factor (VEGF) and its receptors. FASEB journal : official publication of the Federation of American Societies for Experimental Biology. 1999;13(1):9–22. [PubMed: 9872925]
13. Zelzer E, Mamluk R, Ferrara N, Johnson RS, Schipani E, and Olsen BR. VEGFA is necessary for chondrocyte survival during bone development. Development. 2004;131(9):2161–71. [PubMed: 15073147]
14. Thi MM, Iacobas DA, Iacobas S, and Spray DC. Fluid shear stress upregulates vascular endothelial growth factor gene expression in osteoblasts. Annals of the New York Academy of Sciences. 2007;1117:73–81. [PubMed: 17646268]
15. Liu Y, Berendsen AD, Jia S, Lotinun S, Baron R, Ferrara N, et al. Intracellular VEGF regulates the balance between osteoblast and adipocyte differentiation. The Journal of clinical investigation. 2012;122(9):3101–13. [PubMed: 22886301]
16. Lee S, Chen TT, Barber CL, Jordan MC, Murdock J, Desai S, et al. Autocrine VEGF signaling is required for vascular homeostasis. Cell. 2007;130(4):691–703. [PubMed: 17719546]

17. Hu K, and Olsen BR. The roles of vascular endothelial growth factor in bone repair and regeneration. Bone. 2016;91:30–8. [PubMed: 27353702]
18. Geiger F, Lorenz H, Xu W, Szalay K, Kasten P, Claes L, et al. VEGF producing bone marrow stromal cells (BMSC) enhance vascularization and resorption of a natural coral bone substitute. Bone. 2007;41(4):516–22. [PubMed: 17693148]
19. Ferrara N, Gerber HP, and LeCouter J. The biology of VEGF and its receptors. Nature medicine. 2003;9(6):669–76.
20. Bluteau G, Julien M, Magne D, Mallein-Gerin F, Weiss P, Daculsi G, et al. VEGF and VEGF receptors are differentially expressed in chondrocytes. Bone. 2007;40(3):568–76. [PubMed: 17085091]
21. Zelzer E, McLean W, Ng YS, Fukai N, Reginato AM, Lovejoy S, et al. Skeletal defects in VEGF(120/120) mice reveal multiple roles for VEGF in skeletogenesis. Development. 2002;129(8):1893–904. [PubMed: 11934855]
22. Deckers MM, Karperien M, van der Bent C, Yamashita T, Papapoulos SE, and Lowik CW. Expression of vascular endothelial growth factors and their receptors during osteoblast differentiation. Endocrinology. 2000;141(5):1667–74. [PubMed: 10803575]
23. Cross MJ, Dixelius J, Matsumoto T, and Claesson-Welsh L. VEGF-receptor signal transduction. Trends in biochemical sciences. 2003;28(9):488–94. [PubMed: 13678960]
24. Barleon B, Siemeister G, Martiny-Baron G, Weindel K, Herzog C, and Marme D. Vascular endothelial growth factor up-regulates its receptor fms-like tyrosine kinase 1 (FLT-1) and a soluble variant of FLT-1 in human vascular endothelial cells. Cancer Res. 1997;57(23):5421–5. [PubMed: 9393770]
25. Oommen S, Gupta SK, and Vlahakis NE. Vascular endothelial growth factor A (VEGF-A) induces endothelial and cancer cell migration through direct binding to integrin {alpha}9{beta}1: identification of a specific {alpha}9{beta}1 binding site. The Journal of biological chemistry. 2011;286(2):1083–92. [PubMed: 21071450]
26. Deckers MM, van Bezooijen RL, van der Horst G, Hoogendam J, van Der Bent C, Papapoulos SE, et al. Bone morphogenetic proteins stimulate angiogenesis through osteoblast-derived vascular endothelial growth factor A. Endocrinology. 2002;143(4):1545–53. [PubMed: 11897714]
27. Kliche S, and Waltenberger J. VEGF receptor signaling and endothelial function. IUBMB life. 2001;52(1–2):61–6. [PubMed: 11795595]
28. Hu K, and Olsen BR. Osteoblast-derived VEGF regulates osteoblast differentiation and bone formation during bone repair. The Journal of clinical investigation. 2016;126(2):509–26. [PubMed: 26731472]
29. Yang Y-Q, Tan Y-Y, Wong R, Wenden A, Zhang L-K, and Rabie ABM. The role of vascular endothelial growth factor in ossification. International Journal of Oral Science. 2012;4(2):64–8. [PubMed: 22722639]
30. Street J, and Lenehan B. Vascular endothelial growth factor regulates osteoblast survival – evidence for an autocrine feedback mechanism. Journal of Orthopaedic Surgery and Research. 2009;4(1):19. [PubMed: 19527527]
31. Tomlinson RE, McKenzie JA, Schmieder AH, Wohl GR, Lanza GM, and Silva MJ. Angiogenesis is required for stress fracture healing in rats. Bone. 2013;52(1):212–9. [PubMed: 23044046]
32. Street J, Bao M, deGuzman L, Bunting S, Peale FV Jr., Ferrara N, et al. Vascular endothelial growth factor stimulates bone repair by promoting angiogenesis and bone turnover. Proceedings of the National Academy of Sciences of the United States of America. 2002;99(15):9656–61. [PubMed: 12118119]
33. Hankenson KD, Dishowitz M, Gray C, and Schenker M. Angiogenesis in Bone Regeneration. Injury. 2011;42(6):556–61. [PubMed: 21489534]
34. Gerber HP, Vu TH, Ryan AM, Kowalski J, Werb Z, and Ferrara N. VEGF couples hypertrophic cartilage remodeling, ossification and angiogenesis during endochondral bone formation. Nature medicine. 1999;5(6):623–8.
35. Ai-Aql ZS, Alagl AS, Graves DT, Gerstenfeld LC, and Einhorn TA. Molecular mechanisms controlling bone formation during fracture healing and distraction osteogenesis. Journal of dental research. 2008;87(2):107–18. [PubMed: 18218835]

36. Bragdon B, Lam S, Aly S, Femia A, Clark A, Hussein A, et al. Earliest phases of chondrogenesis are dependent upon angiogenesis during ectopic bone formation in mice. Bone. 2017;101:49–61. [PubMed: 28412469]
37. Jacobsen KA, Al-Aql ZS, Wan C, Fitch JL, Stapleton SN, Mason ZD, et al. Bone formation during distraction osteogenesis is dependent on both VEGFR1 and VEGFR2 signaling. J Bone Miner Res. 2008;23(5):596–609. [PubMed: 18433297]
38. Maes C, Kobayashi T, Selig MK, Torrekens S, Roth SI, Mackem S, et al. Osteoblast Precursors, but Not Mature Osteoblasts, Move into Developing and Fractured Bones along with Invading Blood Vessels. Developmental cell. 2010;19(2):329–44. [PubMed: 20708594]
39. Street J, Winter D, Wang JH, Wakai A, McGuinness A, and Redmond HP. Is human fracture hematoma inherently angiogenic? Clinical orthopaedics and related research. 2000(378):224–37.
40. SAHR W, L. M, and B. N. The role of growth factors and related agents in accelerating fracture healing. The Journal of bone and joint surgery British volume. 2006;88-B(6):701–5.
41. Street JT, Wang JH, Wu QD, Wakai A, McGuinness A, and Redmond HP. The angiogenic response to skeletal injury is preserved in the elderly. J Orthop Res. 2001;19(6):1057–66. [PubMed: 11781005]
42. Gerber HP, Hillan KJ, Ryan AM, Kowalski J, Keller GA, Rangell L, et al. VEGF is required for growth and survival in neonatal mice. Development. 1999;126(6):1149–59. [PubMed: 10021335]
43. Ruzankina Y, Pinzon-Guzman C, Asare A, Ong T, Pontano L, Cotsarelis G, et al. Deletion of the developmentally essential gene ATR in adult mice leads to age-related phenotypes and stem cell loss. Cell stem cell. 2007;1(1):113–26. [PubMed: 18371340]
44. Maes C, Kobayashi T, and Kronenberg HM. A novel transgenic mouse model to study the osteoblast lineage in vivo. Annals of the New York Academy of Sciences. 2007;1116:149–64. [PubMed: 18083926]
45. Kim SW, Pajevic PD, Selig M, Barry KJ, Yang JY, Shin CS, et al. Intermittent parathyroid hormone administration converts quiescent lining cells to active osteoblasts. J Bone Miner Res. 2012;27(10):2075–84. [PubMed: 22623172]
46. McKenzie JA, Maschhoff C, Liu X, Migotsky N, Silva MJ, and Gardner MJ. ACTIVATION OF HEDGEHOG SIGNALING BY SYSTEMIC AGONIST IMPROVES FRACTURE HEALING IN AGED MICE. J Orthop Res. 2018.
47. McBride-Gagyi SH, McKenzie JA, Buettmann EG, Gardner MJ, and Silva MJ. Bmp2 conditional knockout in osteoblasts and endothelial cells does not impair bone formation after injury or mechanical loading in adult mice. Bone. 2015;81:533–43. [PubMed: 26344756]
48. Burr DE, Milgrom C (Ed.), Wolinsky I, Martin R, Kawaguchi Y, Beck T, Chisin R, Donahue S, Ekenman I, Finestone A, Mori S, Nunamaker D, Shaffer R, Bennell K, Hulkko A, Yerby S, Egol K, Carter D, Frankel V, Grimston S, Orava S, Vered I, Shemer J, Li J, Friedman E, Schaffler M . Musculoskeletal Fatigue and Stress Fractures. . Boca Raton: CRC Press; 2001.
49. Buettmann EG. Short Communication: Development of an In Vivo Bone Fatigue Damage Model using Axial Compression of the Rabbit Forelimb. 2016;49(14):3564–9.
50. Uthgenannt BA, Kramer MH, Hwu JA, Wopenka B, and Silva MJ. Skeletal Self-Repair: Stress Fracture Healing by Rapid Formation and Densification of Woven Bone. Journal of bone and mineral research : the official journal of the American Society for Bone and Mineral Research. 2007;22(10):1548–56.
51. Liu C, Carrera R, Flamini V, Kenny L, Cabahug-Zuckerman P, George BM, et al. Effects of mechanical loading on cortical defect repair using a novel mechanobiological model of bone healing. Bone. 2018;108:145–55. [PubMed: 29305998]
52. Colnot C Skeletal cell fate decisions within periosteum and bone marrow during bone regeneration. J Bone Miner Res. 2009;24(2):274–82. [PubMed: 18847330]
53. Mizoguchi T, Pinho S, Ahmed J, Kunisaki Y, Hanoun M, Mendelson A, et al. Osterix marks distinct waves of primitive and definitive stromal progenitors during bone marrow development. Developmental cell. 2014;29(3):340–9. [PubMed: 24823377]
54. Dallas SL, and Bonewald LF. Dynamics of the Transition from Osteoblast to Osteocyte. Annals of the New York Academy of Sciences. 2010;1192:437–43. [PubMed: 20392270]

55. Powell WF, Barry KJ, Tulum I, Kobayashi T, Harris SE, Bringhurst FR, et al. Targeted ablation of the PTH/PTHrP receptor in osteocytes impairs bone structure and homeostatic calcemic responses. The Journal of endocrinology. 2011;209(1):21–32. [PubMed: 21220409]
56. Madisen L, Zwingman TA, Sunkin SM, Oh SW, Zariwala HA, Gu H, et al. A robust and high-throughput Cre reporting and characterization system for the whole mouse brain. Nature neuroscience. 2010;13(1):133–40. [PubMed: 20023653]
57. Martinez MD, Schmid GJ, McKenzie JA, Ornitz DM, and Silva MJ. Healing of Non-Displaced Fractures Produced by Fatigue Loading of the Mouse Ulna. Bone. 2010;46(6):1604–12. [PubMed: 20215063]
58. Kim JB, Leucht P, Lam K, Luppen C, Ten Berge D, Nusse R, et al. Bone regeneration is regulated by wnt signaling. J Bone Miner Res. 2007;22(12):1913–23. [PubMed: 17696762]
59. Rossiter H, Barresi C, Pammer J, Rendl M, Haigh J, Wagner EF, et al. Loss of vascular endothelial growth factor a activity in murine epidermal keratinocytes delays wound healing and inhibits tumor formation. Cancer Res. 2004;64(10):3508–16. [PubMed: 15150105]
60. Bustin SA, Benes V, Garson JA, Hellemans J, Huggett J, Kubista M, et al. The MIQE guidelines: minimum information for publication of quantitative real-time PCR experiments. Clinical chemistry. 2009;55(4):611–22. [PubMed: 19246619]
61. Bouxsein ML, Boyd SK, Christiansen BA, Guldberg RE, Jepsen KJ, and Muller R. Guidelines for assessment of bone microstructure in rodents using micro-computed tomography. J Bone Miner Res. 2010;25(7):1468–86. [PubMed: 20533309]
62. Morgan EF, De Giacomo A, and Gerstenfeld LC. Overview of Fracture Healing and Its Assessment. Methods in molecular biology (Clifton, NJ). 2014;1130:13–31.
63. Dempster DW, Compston JE, Drezner MK, Glorieux FH, Kanis JA, Malluche H, et al. Standardized nomenclature, symbols, and units for bone histomorphometry: a 2012 update of the report of the ASBMR Histomorphometry Nomenclature Committee. J Bone Miner Res. 2013;28(1):2–17. [PubMed: 23197339]
64. Shu J, Qiu G, and Mohammad I. 2013 Seventh International Conference on Image and Graphics 2013:937–42.
65. Schindelin J, Arganda-Carreras I, Frise E, Kaynig V, Longair M, Pietzsch T, et al. Fiji: an open-source platform for biological-image analysis. Nature methods. 2012;9:676. [PubMed: 22743772]
66. Utvag SE, Grundnes O, and Reikeraos O. Effects of periosteal stripping on healing of segmental fractures in rats. Journal of orthopaedic trauma. 1996;10(4):279–84. [PubMed: 8723407]
67. Ozaki A, Tsunoda M, Kinoshita S, and Saura R. Role of fracture hematoma and periosteum during fracture healing in rats: interaction of fracture hematoma and the periosteum in the initial step of the healing process. Journal of orthopaedic science : official journal of the Japanese Orthopaedic Association. 2000;5(1):64–70. [PubMed: 10664441]
68. Iwaki A, Jingushi S, Oda Y, Izumi T, Shida JI, Tsuneyoshi M, et al. Localization and quantification of proliferating cells during rat fracture repair: detection of proliferating cell nuclear antigen by immunohistochemistry. J Bone Miner Res. 1997;12(1):96–102. [PubMed: 9240731]
69. Hausman MR, Schaffler MB, and Majeska RJ. Prevention of fracture healing in rats by an inhibitor of angiogenesis. Bone. 2001;29(6):560–4. [PubMed: 11728927]
70. Duan X, Murata Y, Liu Y, Nicolae C, Olsen BR, and Berendsen AD. Vegfa regulates perichondrial vascularity and osteoblast differentiation in bone development. Development (Cambridge, England). 2015;142(11):1984–91.
71. Maes C, Stockmans I, Moermans K, Van Looveren R, Smets N, Carmeliet P, et al. Soluble VEGF isoforms are essential for establishing epiphyseal vascularization and regulating chondrocyte development and survival. The Journal of clinical investigation. 2004;113(2):188–99. [PubMed: 14722611]
72. Holstein JH, Klein M, Garcia P, Histing T, Culemann U, Pizanis A, et al. Rapamycin affects early fracture healing in mice. British journal of pharmacology. 2008;154(5):1055–62. [PubMed: 18454167]
73. Chan C, Seo E, Chen J, Lo D, McArdle A, Sinha R, et al. Identification and specification of the mouse skeletal stem cell. Cell. 2015;160(0):285–298. [PubMed: 25594184]

74. Lu C, Miclau T, Hu D, and Marcucio RS. Ischemia leads to delayed union during fracture healing: a mouse model. J Orthop Res. 2007;25(1):51–61. [PubMed: 17019699]

75. Maes C Placental growth factor mediates mesenchymal cell development, cartilage turnover, and bone remodeling during fracture repair. 2006;116(5):1230–42.

76. Wohl GR, Towler DA, and Silva MJ. Stress Fracture Healing: Fatigue Loading of the Rat Ulna Induces Upregulation in Expression of Osteogenic and Angiogenic Genes that Mimic the Intramembranous Portion of Fracture Repair. Bone. 2009;44(2):320–30. [PubMed: 18950737]

77. Wan C, Gilbert SR, Wang Y, Cao X, Shen X, Ramaswamy G, et al. Activation of the hypoxia-inducible factor-1α pathway accelerates bone regeneration. Proceedings of the National Academy of Sciences of the United States of America. 2008;105(2):686–91. [PubMed: 18184809]

78. Brownlow HC, Reed A, and Simpson AH. The vascularity of atrophic non-unions. Injury. 2002;33(2):145–50. [PubMed: 11890916]

A

Mouse Genotype	Abbreviation
UBC-CreERT2$^{-/-}$; VEGFA$^{fl/fl}$; Ai9$^{+/-}$	UBC Control
UBC-CreERT2$^{+/-}$; VEGFA$^{fl/fl}$; Ai9$^{+/-}$	UBC cKO
Osx-CreERT2$^{-/-}$; VEGFA$^{fl/fl}$; Ai9$^{+/-}$	Osx Control
Osx-CreERT2$^{+/-}$; VEGFA$^{fl/fl}$; Ai9$^{+/-}$	Osx cKO
Dmp1-CreERT2$^{-/-}$; VEGFA$^{fl/fl}$; Ai9$^{+/-}$	Dmp1 Control
Dmp1-CreERT2$^{+/-}$; VEGFA$^{fl/fl}$; Ai9$^{+/-}$	Dmp1 cKO

B

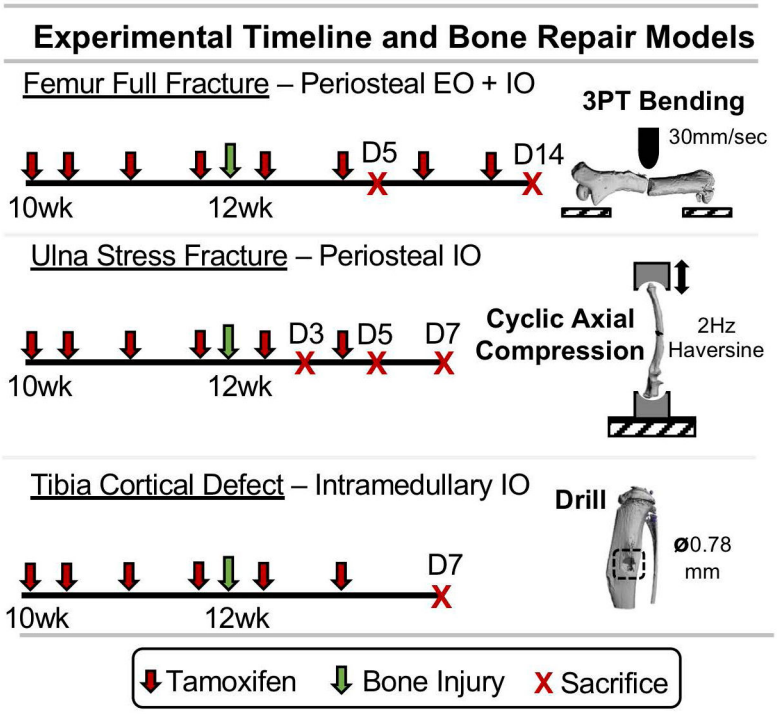

Figure 1. Experimental overview of mouse lines and models of bone repair.

A) All bone injury experiments used female and male mice from three different genetic backgrounds carrying VEGFA floxed (VEGFA $^{fl/fl}$) and tdTomato (Ai9$^{+/-}$) alleles. Mice containing UBC, Osx, or Dmp1 inducible Cre transgenes (CreERT2$^{+/-}$) served as Cre specific VEGFA inducible conditional knock-out (cKO) animals. Littermate mice from the same genetic background not harboring Cre (CreERT2$^{-/-}$) served as control animals. **B)** All mice received tamoxifen (2x weekly; red arrow) by oral gavage (100 mg/kg) starting 2 weeks before injury. Mice had bone injuries induced at 12 weeks of age (green arrow) by 3-point bending of the femur (full fracture), cyclic axial compression of the ulna (stress fracture), or tibia drilling (cortical defect). Full fracture induced periosteal bone formation by endochondral ossification (EO) and intramembranous ossification (IO). Stress fracture and cortical defect induced bone formation by periosteal or intramedullary IO, respectively. Mice were sacrificed at predefined timepoints (red X).

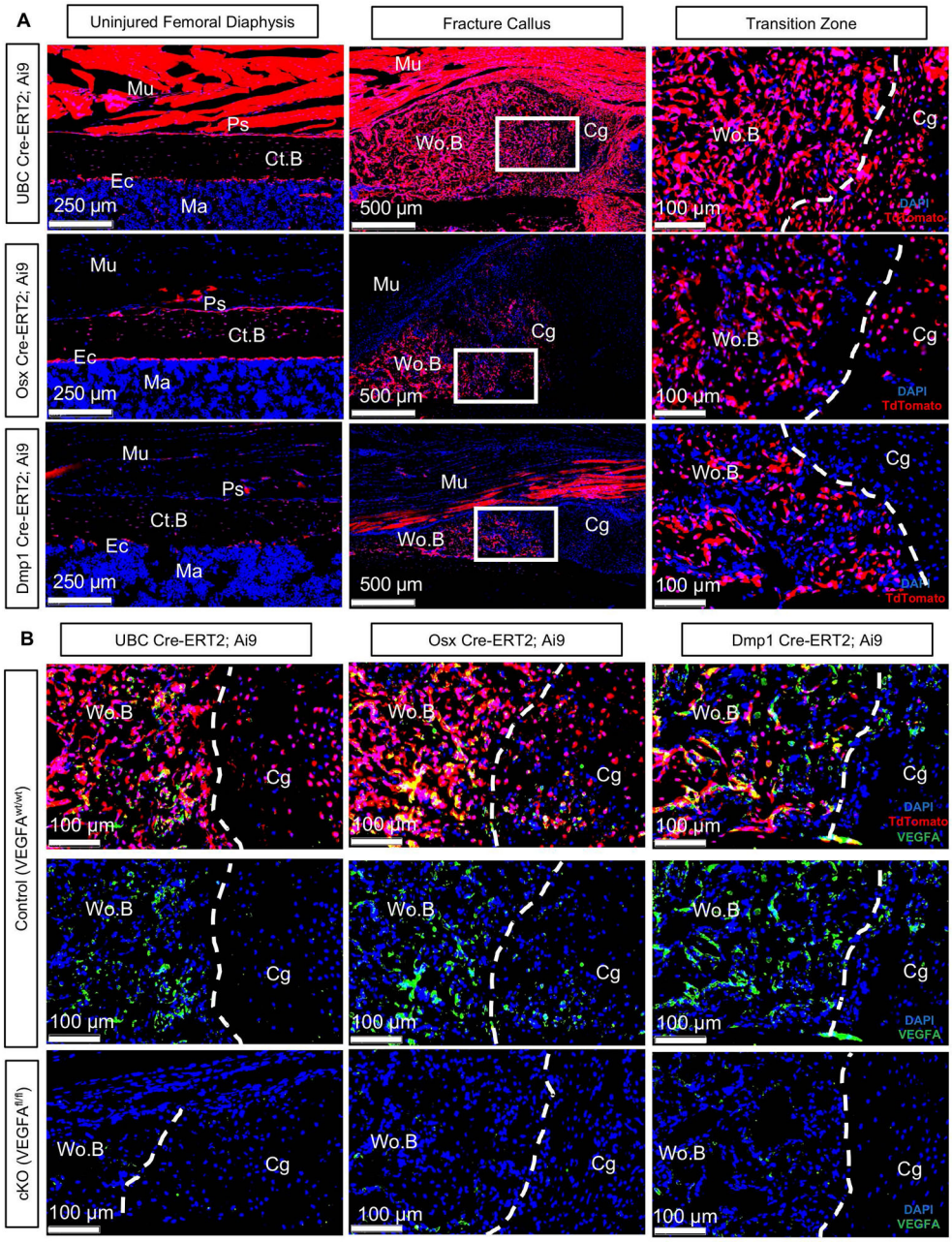

Figure 2. Inducible Cre lines spatial targeting and VEGFA deletion in fracture callus.

A) TdTomato reporter images (20x) counterstained with DAPI demonstrate spatial inducible Cre activation in Cre-ERT2 Ai9 VEGFA$^{wt/wt}$ mice following tamoxifen schedule as shown in Figure 1B. tdTomato expression from the midpoint of intact diaphyseal bone (femur). UBC targets periosteum and marrow cells. Osx targets most of periosteum but no marrow. Dmp1 targets some periosteum and no marrow. Day 14 full fracture tdTomato reporter images (5x). UBC targets muscle and all callus tissues. Osx targets woven bone and some cartilage in callus. Dmp1 targets woven bone and muscle. White box shows magnified view (20x) of transition zone; the part of fracture callus where cartilage is undergoing endrochondral ossification to become woven bone. Ps = Periosteal Surface; Ec =

Endocortical Surface; Mu = Skeletal Muscle; Ct.B = cortical bone; Ma = marrow. Wo.B = woven bone; Cg = cartilage. **B)** Fluorescent immunostained femur fracture sections from control Ai9 mice ($VEGFA^{wt/wt}$) show that VEGFA (Alexa-488 signal) protein is predominantly localized in woven bone (Wo.B) regions of the callus near UBC, Osx and Dmp1 Cre activated woven bone lining osteoblasts. VEGFA is also localized near chondrocytes that show UBC and Osx Cre activation. UBC, Osx, and Dmp1 cKO calluses show less VEGFA protein expression in woven bone regions than respective control calluses.

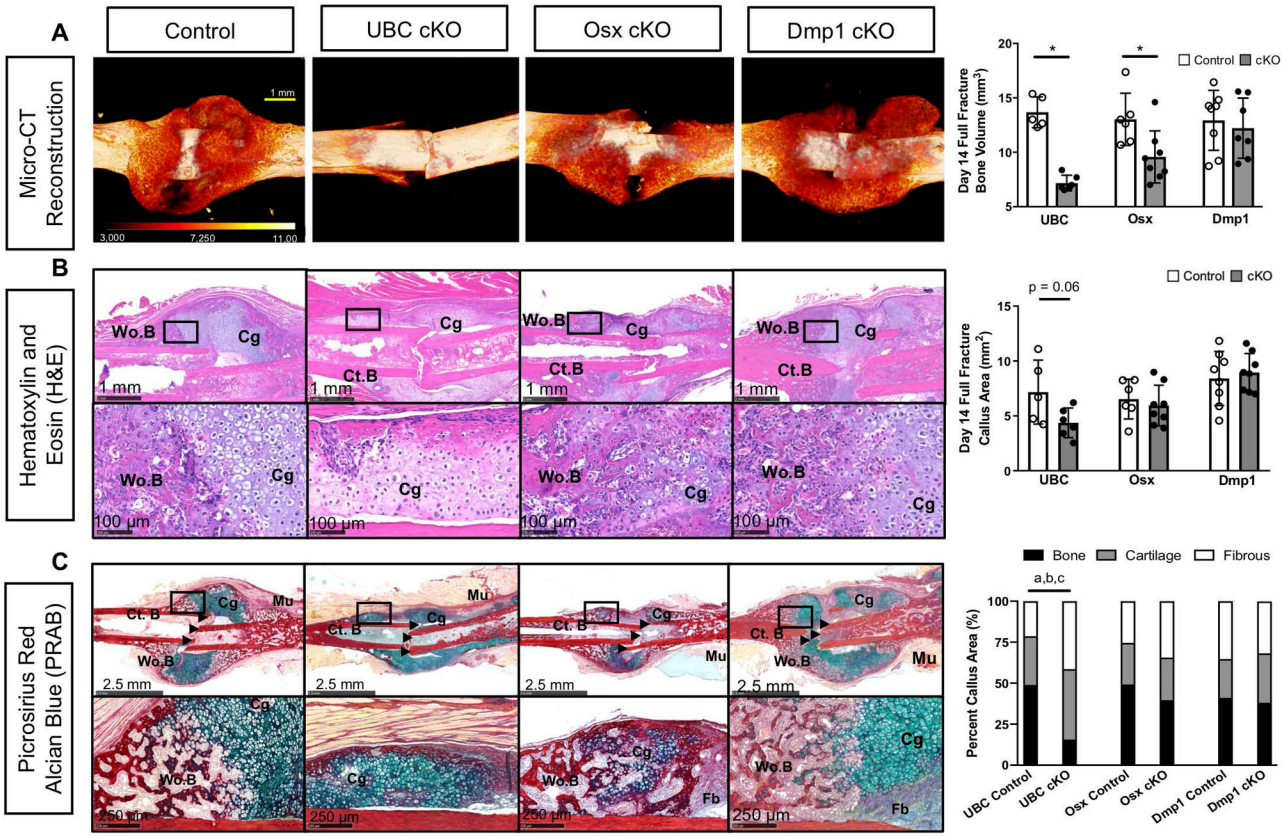

Figure 3. Deletion of VEGFA ubiquitously and in early (Osx+) but not later (Dmp1+) osteolineage cells impaired periosteal bone formation after full fracture.

A) 3D reconstruction of analyzed bone volume for each Cre line depicted with heat map based on degree of mineralization. UBC cKO full fractured femurs showed minimal appreciable woven bone. Osx cKO full fractured femurs showed impaired woven bone formation. DMP1 cKO full fractured femurs showed comparable woven bone formation to controls. Thresholded bone volume of full fracture microCT calluses after 14 days of healing showed impaired bone formation in UBC cKO and Osx cKO mice versus controls (unpaired t-test; * $p<0.05$). Bone metrics were quantified from 600 slices (6.3 mm) at 10.5 micron resolution centered around the fracture midpoint including the original cortical bone (Supplemental Figure 3A). As a result the y-axis begins at 5 mm^3, which is the average bone volume from intact (non-fractured) femurs from all 3 inducible Cre lines. There were no significant differences in bone volume between femurs from non-fractured Cre lines (Supplemental Table 3). **B)** Hematoxylin and Eosin (H&E) day 14 sagittal sections from the fracture midpoint to show callus cellularity and size. Black box shows a magnified (20x) view of the transition zone. UBC cKO fracture calluses trended toward having a smaller callus area versus controls ($p =0.06$). Osx cKO and Dmp1 cKO fracture calluses weren't significantly smaller. **C)** Serial picrosirius red alcian blue day 14 sagittal sections from the fracture midpoint. Control mice displayed a mixture of woven bone (Wo.B; red stain) around the periphery of the fracture site (black arrow heads) and cartilage (Cg; blue stain) near the fracture site. UBC cKO femurs displayed as a percentage of total callus area significantly less (a $p <0.05$) woven bone and significantly more cartilage (b $p <0.05$) and fibrous tissue

(c $p < 0.05$). Osx cKO femurs had calluses with less woven bone present but this wasn't significant when normalized to callus area. Dmp1 cKO femurs had comparable composition compared to controls.

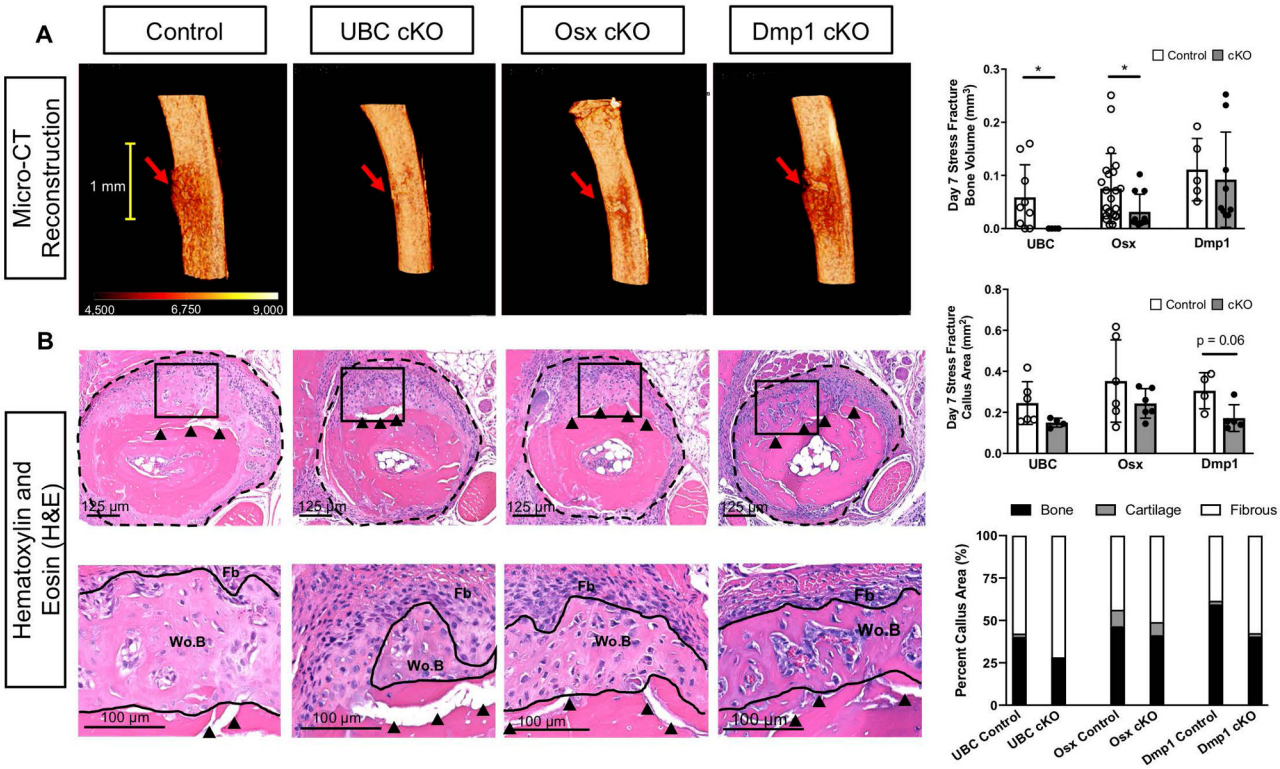

Figure 4. Deletion of VEGFA ubiquitously and in early (Osx+) but not later (Dmp1+) osteolineage cells impaired periosteal bone formation after stress fracture.

A) 3D reconstruction of analysis region shows representative bone formation for each Cre line around stress fracture site (red arrow). UBC cKO stress fractured ulnae showed no quantifiable woven bone via micro-CT. Osx cKO stress fractured ulnae showed impaired woven bone extent and volume. DMP1 cKO stress fractured ulnae showed comparable bone formation to controls. Thresholded bone volume (BV) for entire periosteal callus tissue (which excludes intact cortical bone; Supplemental Figure 3B) on day 7 after stress fracture showed impaired bone formation in UBC cKO and Osx cKO mice versus controls (unpaired t-test; * $p<0.05$). **B)** Hematoxylin and Eosin (H&E) transverse sections taken near the crack site (red arrow) of day 7 post stress fractured ulnae displayed a region of woven bone (Wo.B) and expanded fibrous periosteum (Fb; dashed black line) around the stress fracture crack (black arrow heads) for all Cre lines. Quantification of this expanded periosteum area showed that Dmp1 cKO stress fracture calluses trended toward being smaller ($p = 0.06$) versus controls. UBC and Osx cKO calluses weren't significantly different in size versus controls. Woven bone (Wo.B), cartilage (Cg) and fibrous (Fb) tissue areas were quantified at higher magnification (Black Box - 20x) and normalized to callus area. No cKO stress fracture calluses had a significantly altered callus composition compared to controls across all Cre lines. Note the minimal amount of cartilage in the stress fracture model.

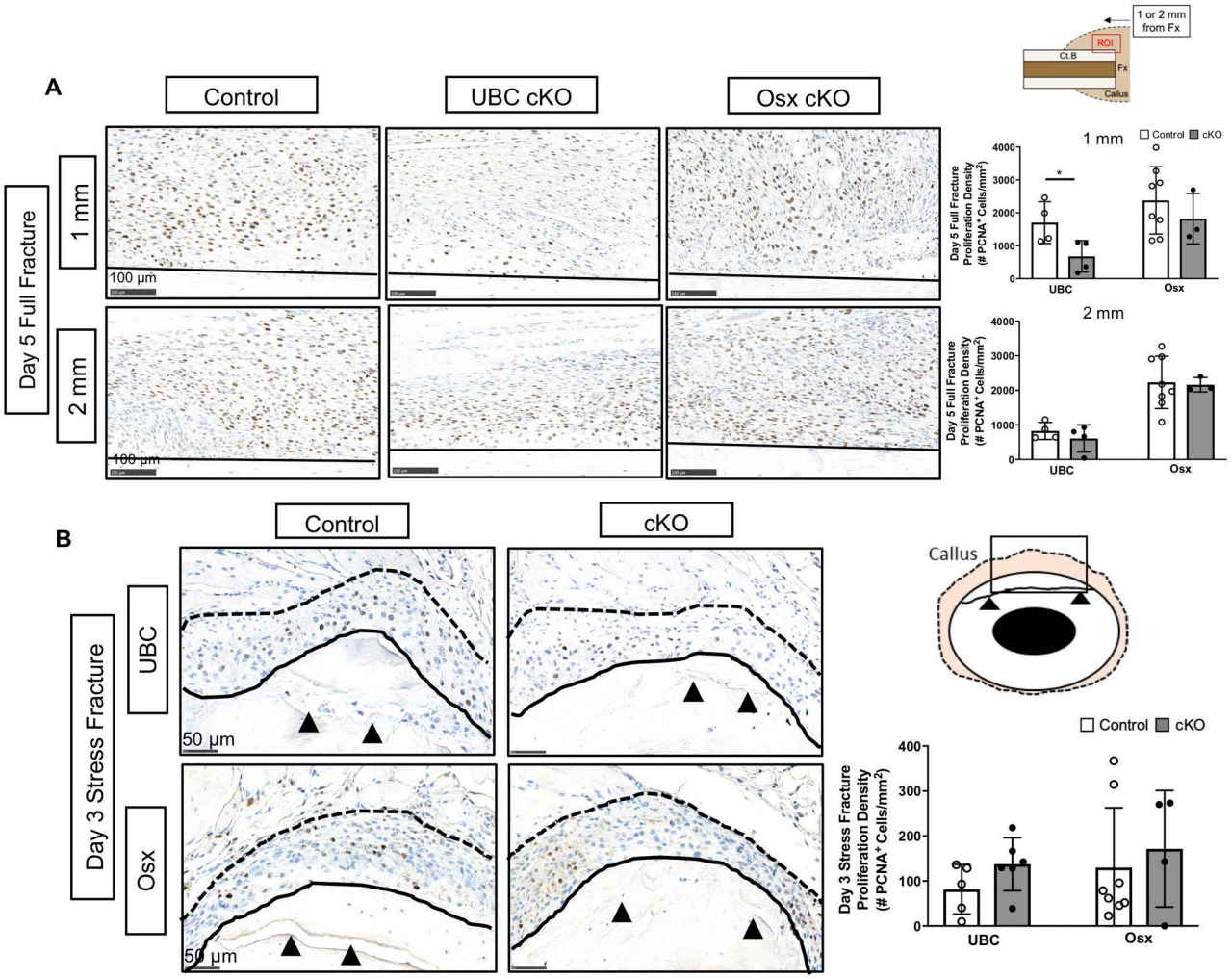

Figure 5. Deletion of VEGFA ubiquitously but not in early (Osx+) osteolineage cells impaired periosteal proliferation after fracture.

A) Representative day 5 full fracture PCNA stained images (20x) of the expanded periosteum at sites 1 mm and 2 mm from the fracture site. The ROI consisted of the region above the cortical bone (black solid line) in each image. PCNA staining of the expanded periosteum 1 mm from the full fracture site revealed a significant reduction in the periosteal proliferative density (# $PCNA^+$ cells/expanded periosteal area) following UBC cKO but not Osx cKO of VEGFA at day 5 (2-Way ANOVA with Sidak Post Hoc Test (* = $p < 0.05$)). A field of view 2 mm from the full fracture site demonstrated no differences between groups in proliferation density. **B)** Representative day 3 stress fracture PCNA stained images (40x) showing an enhanced view around the fracture site (black arrows). Stress fracture PCNA staining of the entire expanded periosteum (area between solid black line and dotted black line) after 3 days revealed no reduction in the proliferative density following VEGFA deletion.

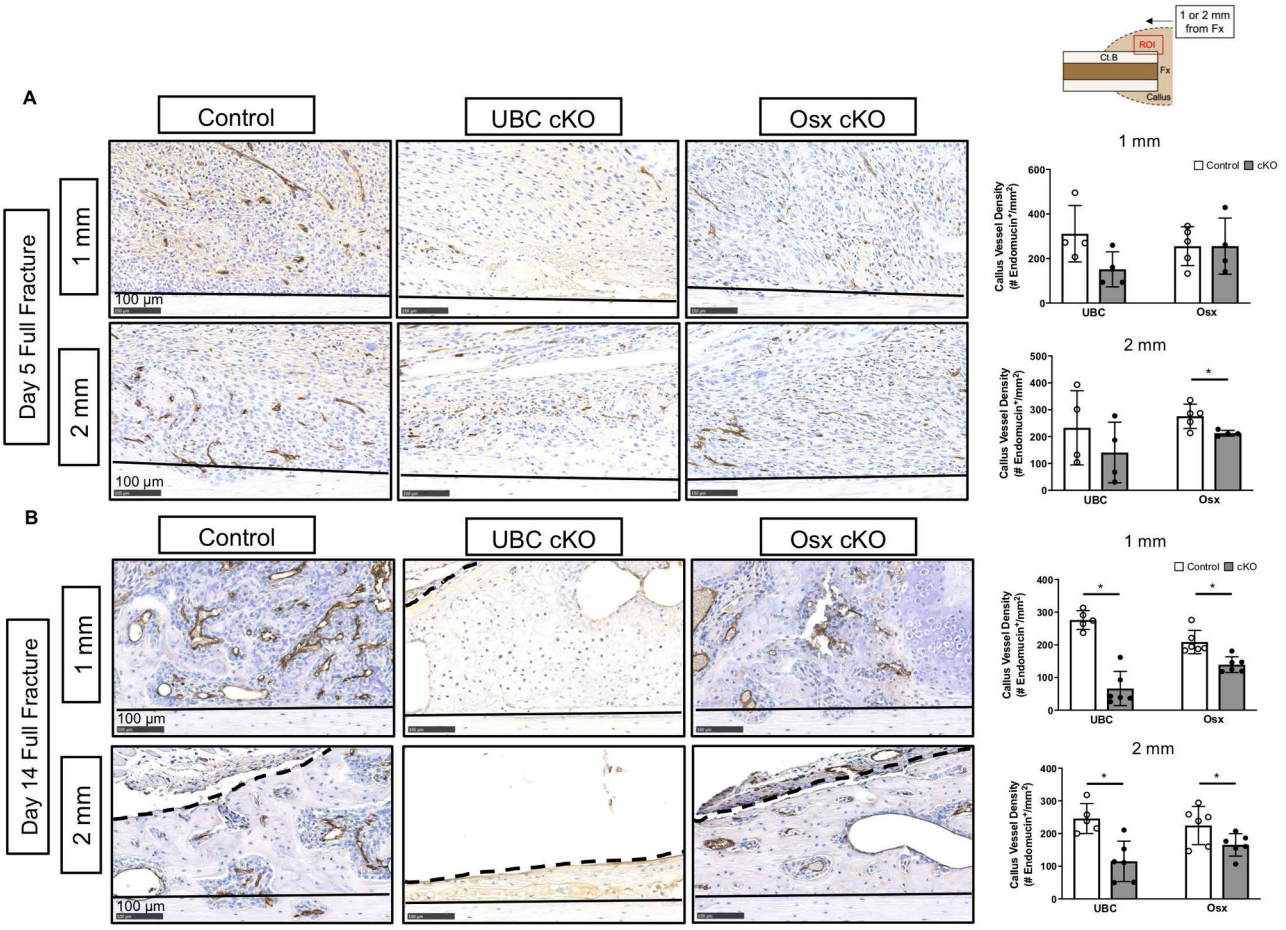

Figure 6. Deletion of VEGFA ubiquitously and in early (Osx+) osteolineage cells impairs periosteal angiogenesis following full fracture.

A) Representative endomucin stained images (20x) of the expanded periosteum at day 5 following full fracture. The ROI consisted of a region between the cortical bone (black solid line) and periphery of the callus near the skeletal muscle (dashed black line). At day 5, endomucin staining of the expanded periosteum 1 mm and 2 mm from the full fracture site revealed no significant changes in periosteal vessel density (# endomucin^{+}/expanded periosteal area) due to loss of VEGFA (2-Way ANOVA with Sidak Post Hoc Test). **B)** Representative endomucin stained images (20x) at day 14 following fracture however show a dramatic loss of vascular infiltration in UBC cKO callus tissue and a less severe loss in Osx cKO femurs at locations 1 mm from the fracture site. Similar results were found within woven bone fields of view 2 mm from the full fracture site. At 14 days, endomucin staining of callus tissue 1 mm and 2 mm from the full fracture site revealed significant reductions in vessel density in UBC cKO and Osx cKO mice (2-Way ANOVA with Sidak Post Hoc Test; * $p < 0.05$).

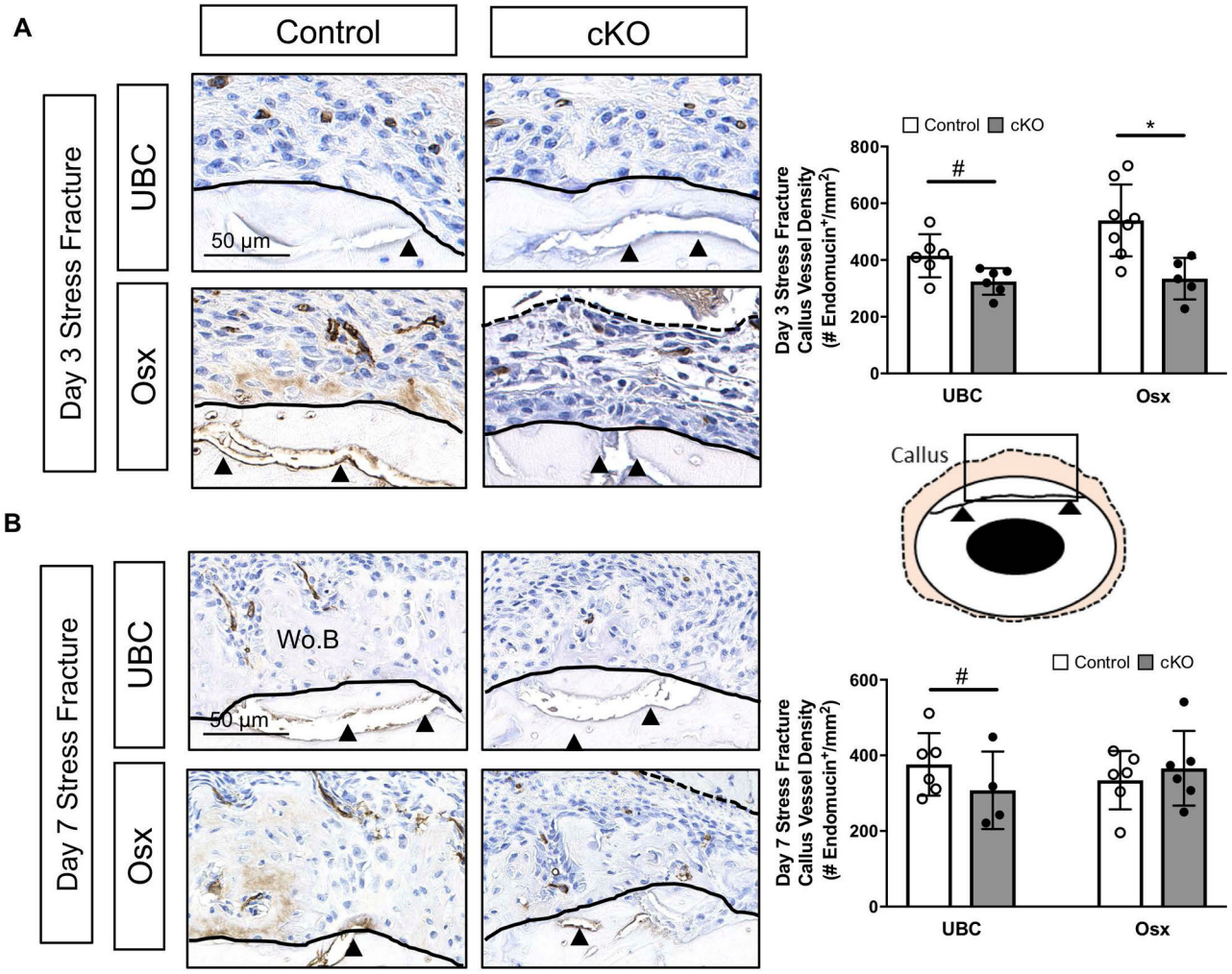

Figure 7. Deletion of VEGFA ubiquitously and in early (Osx+) osteolineage cells impairs periosteal angiogenesis following stress fracture.

A) Representative day 3 endomucin stained images (40x) highlight the region around the stress fracture crack (black arrow heads). The ROI (tan region on schematic) consisted of the expanded periosteal region between the cortical bone (black solid line) and skeletal muscle (dashed black line). Note the absence of appreciable woven bone in all groups at day 3. Endomucin staining quantification of the ROI between genotypes at various timepoints (days 3, 5, 7) revealed a significant decrease in periosteal vessel density (# endomucin$^+$/ expanded periosteal area) due to genotype in UBC cKO (2-Way ANOVA, # $p<0.05$ for genotype) and only at day 3 due to genotype in Osx cKO mice (Sidak Post Hoc Test, * $p< 0.05$). **B)** Representative day 7 endomucin stained images (40x) highlight the region around the stress fracture crack (black arrow heads). At day 7, there is now woven bone (Wo.B) infiltrated with blood vessels within the periosteal space. Callus vessel density of the periosteal ROI (# endomucin$^+$/expanded periosteal area) at day 7 (2 way ANOVA; # p-value < 0.05 for genotype).

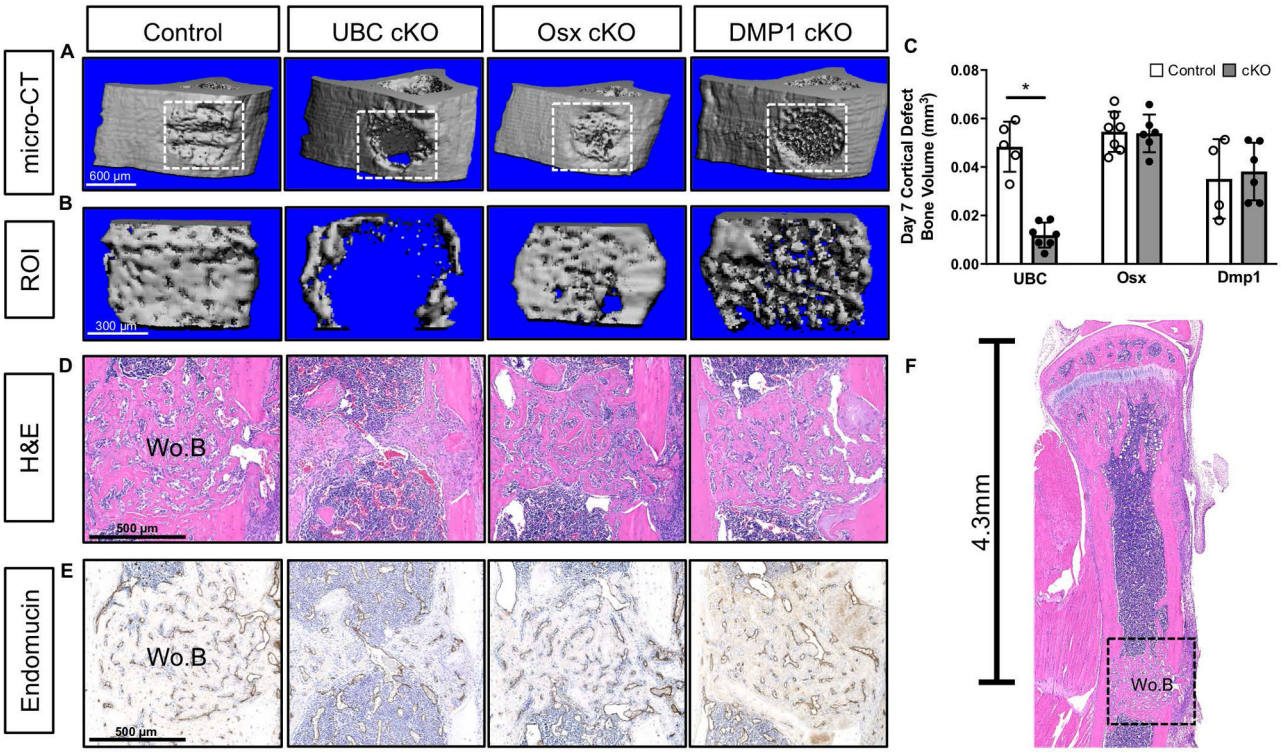

Figure 8. Deletion of VEGFA ubiquitously but not in early (Osx+) or late (Dmp1+) osteolineage cells impaired cortical defect repair.

A) 3D reconstruction of representative tibiae with defect site (white box) for each Cre line shows that only UBC cKO mice failed to fill in the cortical defect by day 7. **B)** Reconstruction of thresholded bone tissue that was quantified within the defect site. **C)** Thresholded bone volume (BV) of cortical defect site using microCT after 7 days of healing showed impaired bone formation in UBC cKO cortical defects versus controls (unpaired t-test; *$p<0.05$). Bone metrics were quantified from 55 slices (0.58 mm) at 10 micron resolution centered around the drill site which excluded original intact cortical bone (Supplemental Figure 3C). **D)** Magnified H&E section (10x) depicting woven bone formation (Wo.B) at the defect site for each specimen represented in panels A and B. **E)** Endomucin stained serial sections from panel D that show the co-occurrence of vasculature at sites of woven bone formation. **F)** Hematoxylin and Eosin (H&E) sagittal sections depicting location of defect site (4.3 mm) and subsequent woven bone formation (Wo.B; black dashed box) 7 days after injury. Note how local the response is and the absence of large amounts of periosteal woven bone.

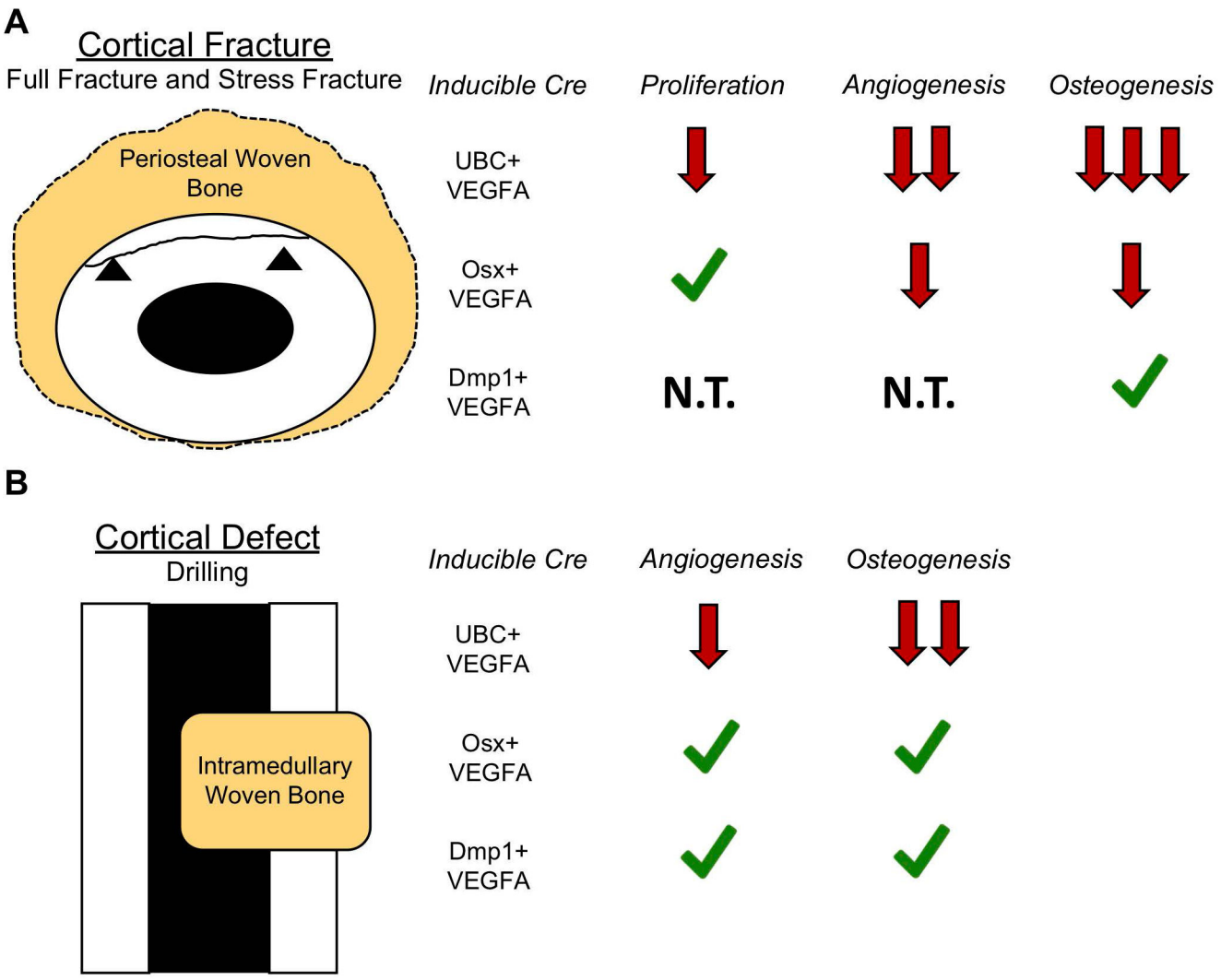

Figure 9. Graphical summaries of the results from full fracture, stress fracture and cortical defect models.

A) Each of the VEGFA results are put into the context of normal fracture repair, that requires periosteal proliferation, angiogenesis, and osteogenesis for healing. Loss of UBC+ cell VEGFA leads to dramatically impaired periosteal angiogenesis and osteogenesis and to a lesser extent impaired cellular proliferation which prevents successful bone healing. Loss of Osx+ cell VEGFA but not Dmp1+ cell VEGFA prevents periosteal angiogenesis and osteogenesis thereby leading to reductions in maximal bone formation. **B)** UBC+ cell VEGFA was required for maximal angiogenesis and osteogenesis for cortical defect repair. VEGFA from Osx+ or Dmp1+ cells was dispensable for angiogenesis and osteogenesis for cortical defect repair. Green check = Cell source of VEGFA dispensable for biological process; Red arrows = cell source of VEGFA required for biological process. **N.T.** = not tested.